UNIVERSITY OF JYVÄSKYLÄ
DEPARTMENT OF CHEMISTRY
RESEARCH REPORT No. 123

QUANTUM CHEMICAL CALCULATIONS OF STRUCTURES, BONDING, AND SPECTROSCOPIC PROPERTIES OF SOME SULFUR AND SELENIUM IODINE CATIONS

BY

J. MIKKO RAUTIAINEN

Academic Dissertation
for the Degree of
Doctor of Philosophy

Jyväskylä, Finland
2007

DEPARTMENT OF CHEMISTRY, UNIVERSITY OF JYVÄSKYLÄ
RESEARCH REPORT No. 123

QUANTUM CHEMICAL CALCULATIONS OF STRUCTURES, BONDING, AND SPECTROSCOPIC PROPERTIES OF SOME SULFUR AND SELENIUM IODINE CATIONS

BY

J. MIKKO RAUTIAINEN

Academic Dissertation
for the Degree of
Doctor of Philosophy

To be presented, by permission of the Faculty of Mathematics and Natural Sciences of the University of Jyväskylä, for public examination in Auditorium KEM4, on December 5th, 2007, at 12 noon.

Jyväskylä, Finland
ISBN 978-951-39-2984-8
ISSN 0357-346X

URN:ISBN:978-952-86-0121-0
ISBN 978-952-86-0121-0 (PDF)
ISSN 0357-346X

University of Jyväskylä, 2024

ABSTRACT

The characterization and understanding of electronic structures of sulfur and selenium iodine species have presented many difficulties, some of which have puzzled scientists for decades. The present thesis provides answers to some of the open questions with the aid of modern quantum chemical tools.

The research presented in the first half of this thesis describes the bonding in several sulfur and selenium iodine cations, which is of interest because many of the structures display unconventional bonding arrangements and because sulfur and selenium iodine cations are an exception to the normal trend that elements within the same group exhibit similar bonding with other elements. So far the only unequivocally characterized sulfur and selenium iodine cations that even have the same formula are $S_2I_4^{2+}$ and $Se_2I_4^{2+}$, and even their structures are fundamentally different. The investigation of the bonding in $S_2I_4^{2+}$ and $Se_2I_4^{2+}$ reveals that the different structures arise from the intricate balance between the strengths of homoatomic and heteroatomic π and σ bonds. The non-existence of SI_3^+ compared to experimentally observed SeI_3^+ is shown to arise from their different stabilities with respect to the formation of $E_2I_4^{2+}$ (E = S, Se) dications in solution. These results provide a basis for the study of the stabilities of larger sulfur and selenium iodine cations in different phases and for the exploration of more general reasons why the cations appear to adopt different structures.

The theoretical bonding analyses also confirm the validity of simple π^*- π^* bonding and charge delocalization models that have been used to explain the unconventional bonding observed in cationic sulfur and selenium species. The validation of the π^*- π^* bonding description gives theoretical justification for its use in describing various multi-center bonding situations presented in recent literature.

The second half of the thesis summarizes the requirements for producing accurate and computationally feasible theoretical predictions of ^{77}Se NMR chemical shifts for selenium iodine species in solution. The consideration of relativistic and solvent effects together with the use of efficient DFT methods is shown to facilitate the calculation of ^{77}Se chemical shifts with sufficient accuracy for them to be helpful in the identification of unknown species. The theoretical calculations are utilized together with NMR spectroscopic measurements to identify selenium iodine cations present in the equilibrium solution of the reversible dissociation of $(Se_6I_2)[AsF_6]_2$ in SO_2. These new cations provide a significant addition to the group of selenium iodine species. They can be used in further studies to elucidate the understanding of the bonding and factors that lead to the different structures observed in different phases. The computational methods and requirements reviewed and employed in this thesis can be readily applied to the prediction of the chemical shifts of other NMR active heavy elements.

Author's address

J. Mikko Rautiainen
Department of Chemistry
University of Jyväskylä
P.O. Box 35
40014 University of Jyväskylä
Finland
mirauta@jyu.fi

Supervisors

Professor Jussi Valkonen
Department of Chemistry
University of Jyväskylä
Finland

Professor Risto Laitinen
Department of Chemistry
University of Oulu
Finland

Professor Jack Passmore
Department of Chemistry
University of New Brunswick
Canada

Docent Reijo Suontamo
Department of Chemistry
University of Jyväskylä
Finland

Reviewers

Professor Kari Laasonen
Department of Chemistry
University of Oulu
Finland

Professor Matti Hotokka
Department of Physical Chemistry
Åbo Akademi University
Finland

Opponent

Professor Tapani Pakkanen
Department of Chemistry
University of Joensuu
Finland

PREFACE

The work presented in this thesis has been carried out at the Departments of Chemistry, University of Jyväskylä and University of New Brunswick from spring 2002 to autumn 2007.

I wish to express my warmest gratitude to my supervisors Professors Jussi Valkonen, Risto Laitinen (University of Oulu), and Jack Passmore (University of New Brunswick) as well as Docent Reijo Suontamo for giving me the opportunity to undertake this research and introducing me to the interesting world of chalcogen halogen chemistry. Without their patient guidance, support and encouragement during the past years none of this work would have been possible.

My sincere thanks go to Dr. Heikki Tuononen for talking me into this project, for his help with the numerous theoretical and practical issues that I've faced during these years, and for keeping our computers running smoothly. I am also indebted to Dr. Carsten Knapp for his critical views that stopped me from making a fool of myself more than once and for his role as the co-ordinator who kept everybody on the same page during the research projects. I would like to acknowledge the referees of this thesis Professors Kari Laasonen (University of Oulu) and Matti Hotokka (Åbo Akademi University) for their valuable criticism and Professor Emeritus Matti Nurmia for revising the language of this thesis. My special thanks go to all the people at the Laboratory of Inorganic and Analytical Chemistry for creating a pleasant and inspiring working environment. I also wish to express my gratitude to everybody at the Passmore Research Group for all their help and kindness during my stay in Fredericton.

I wish to thank my parents and brothers for their continued support over the years and for letting me find my own way in life. My thanks are also due to all of my friends in- and outside of the Chemistry Department who have made my days brighter and given me the strength to complete this work.

Finally, I gratefully acknowledge the financial support from the Ministry of Education in Finland (Chemistry Graduate Program of Inorganic Materials) and Helsingin Sanomain 100-vuotissäätiö, as well as the computing resources provided by the Scientific Computing Ltd.

Jyväskylä, November 13th 2007

Mikko Rautiainen

LIST OF ORIGINAL PUBLICATIONS

The main results of this thesis are based on the following original research papers, which are referred to in the text by their Roman numerals.

I **The Highest Bond Order Between Heavier Main-Group Elements in an Isolated Compound? Energetics and Vibrational Spectroscopy of $S_2I_4(MF_6)_2$ (M = As, Sb)**, Scott Brownridge, T. Stanley Cameron, Hongbin Du, Carsten Knapp, Ralf Koeppe, Jack Passmore, J. Mikko Rautiainen, and Hansgeorg Schnöckel, *Inorg. Chem.* **2005**, *44*, 1660-1671.
https://doi.org/10.1021/ic049035g

II **Accounting for the Differences in the Structures and Relative Energies of the Highly Homoatomic np_π - np_π (n ≥ 3) Bonded $S_2I_4^{2+}$, the Se-I π Bonded $Se_2I_4^{2+}$, and Their Higher Energy Isomers by AIM, MO, NBO, and VB Methodologies**, Scott Brownridge, Margaret-Jane Crawford, Hongbin Du, Richard D. Harcourt, Carsten Knapp, Risto S. Laitinen, Jack Passmore, J. Mikko Rautiainen, Reijo J. Suontamo, and Jussi Valkonen, *Inorg. Chem.* **2007**, 46, 681-699
https://doi.org/10.1021/ic061523w

III **A Computational and Experimental Study of the Structures and Raman and ^{77}Se NMR Spectra of SeX_3^+ and SeX_2 (X = Cl, Br, I): FT-Raman Spectrum of $(SeI_3)[AsF_6]$**, J. Mikko Rautiainen, Todd Way, Gabriele Schatte, Jack Passmore, Risto S. Laitinen, Reijo J. Suontamo, and Jussi Valkonen, *Inorg. Chem.* **2005**, *44*, 1904-1913.
https://doi.org/10.1021/ic048310w

IV **^{77}Se NMR Spectroscopic and DFT MO Investigation of the Reversible Dissociation of $(Se_6I_2)[AsF_6]_2$ in Liquid SO_2**, Scott Brownridge, Larry Calhoun, Risto S. Laitinen, Michael Murchie, Jack Passmore, Jarkko Pietikäinen, J. Mikko Rautiainen, Jeremy C. P. Sanders, Gary J. Schrobilgen, Reijo J. Suontamo, Jussi U. Valkonen, and Chi-Ming Wong, manuscript.
https://doi.org/10.1021/ic8015673

The author of the present thesis has done all the computational work in publications **I-IV**, apart from the normal coordinate analysis and some low level calculations in Paper **I** and the valence bond analysis in Paper **II**. The author has written a part of Paper **I**, co-written Paper **IV**, and has been the principal writer in Papers **II** and **III**.

ABBREVIATIONS

AIM	Atoms in molecules theory
ANO	Atomic natural orbital
BCP	Bond critical point
B3PW91	Becke three parameter exchange functional with Perdew-Wang 91 correlation functional
COSMO	Conductor-like screening model
COSY	Correlation spectroscopy
CSGT	Continuous set of gauge transformations
DFT	Density functional theory
DKH2	Second order Douglas-Kroll-Hess approximation
ECP	Effective core potential
FT	Fourier transformation
GGA	Generalized gradient approximation
GIAO	Gauge-including atomic orbital
HAHA	Heavy atom effect on heavy atom
HALA	Heavy atom effect on light atom
HF	Hartree-Fock
HOMO	Highest occupied molecular orbital
IGAIM	Individual gauges for atoms in molecules
IGLO	Individual gauge for localized orbitals
LDA	Local density approximation
LORG	Localized orbitals/localized origins
MO	Molecular orbital
MP2	Second order Møller-Plesset theory
MPW1PW91	Modified Perdew-Wang exchange functional with Perdew-Wang 91 correlation functional
NAO	Natural atomic orbital
NBO	Natural bond orbital
NMR	Nuclear magnetic resonance
PBE0	Hybrid version of Perdew, Burke and Ernzerhof functional
ppm	Parts per million
PS-DQF	Phase-sensitive Double-Quantum-Filtered
rPBE	Revised version of generalized gradient approximation functional of Perdew, Burke and Ernzerhof
SDB	Stuttgart-Dresden-Bonn effective core potential
SOMO	Singly occupied molecular orbital
STO	Slater type orbital
VB	Valence bond
VSEPR	Valence shell electron pair repulsion theory
ZORA	Zeroth order regular approximation

CONTENTS

1 INTRODUCTION

Binary sulfur iodine and selenium iodine species were once thought to be essentially non-existent.[1] Since then several, mainly cationic, species have been characterized.[2] Many of the structures that sulfur and selenium iodine cations adopt are not readily predicted by the simple valence shell electron pair repulsion (VSEPR) theory or explained by the classical electron precise Lewis bonding approach.[3] Consequently, they provide a good opportunity for the development of bonding models and increasing the understanding of bonding in general.

The first half of the present study concentrates on the investigation of the bonding in these fascinating sulfur and selenium iodine cations. The previous studies have introduced concepts such as stabilization through delocalization of charges or π^*- π^* bonds to explain the observed structures.[2] The motivation for the current study has been to use the tools provided by quantum chemistry to examine the bonding in these cations and to test how the proposed concepts hold when compared to more universal bonding theories such as natural bond orbital theory.[4] Another objective for studying the bonding has been to find reasons why sulfur and selenium iodine cations exhibit fundamentally different structures in the solid state. A specific case study focuses on the differences in $S_2I_4^{2+}$ and $Se_2I_4^{2+}$, because so far they are the only structurally characterized sulfur and selenium iodine ions that have the same formula.[2]

The second half of the thesis describes how quantum chemical methods can be applied to the prediction of ^{77}Se NMR chemical shifts. NMR spectroscopy is a powerful method and it provides a lot of information that can be used for the identification and characterization of new species in solution and other phases. The interpretation of NMR information can be greatly aided by theoretical calculations of NMR parameters. However, the accurate theoretical prediction of NMR parameters is not a trivial task at least for elements beyond the second row of the periodic table, and the methods used for the calculation of NMR parameters are still undergoing development.[5] The performance of different NMR calculation methods in reproducing the experimental ^{77}Se chemical shifts of well characterized selenium species is

tested and requirements for the calculation of ^{77}Se chemical shifts with a reasonable accuracy are established. Quantum chemical calculations are then applied to aid the identification of the unknown selenium species observed in the equilibrium solution of the reversible dissociation of $(Se_6I_2)[AsF_6]_2$ in SO_2.

2 STRUCTURES AND BONDING OF CHALCOGEN IODINE COMPOUNDS

2.1 Introduction to bonding models

The most common way for chemists to describe chemical species is in terms of atoms held together by bonds. The atoms and bonds form the foundation for conceptual models that are used to explain and predict chemical structures and their behavior. The conceptual bonding models include for example VSEPR theory, Lewis structures, and their extensions that have been derived to describe bonding situations for which the original theories have proved inadequate.

In contrast to the conceptual models, quantum chemical methods describe molecules by wavefunctions defined in terms of positive nuclei surrounded by a cloud of negative electrons. The discrepancy in the way the quantum chemical methods and chemists describe chemical species often causes difficulties in interpreting the results of the calculations. Various theoretical models have been developed in order to bridge the gap between the conceptual models and the quantum chemical results. These theoretical models are based on a mathematical analysis of wavefunctions or electron densities (experimental or calculated). Wavefunction analysis methods mainly include different orbital localization schemes. Natural bond orbital analysis is a well known example of a method based on the localization of orbitals.[4] Two of the most widely used methods to analyze electron densities are the theory of atoms in molecules by Bader [6] and the analysis of the electron localization function.[7] In the next two sections, the natural bond orbital analysis and the theory of atoms in molecules are introduced more closely.

2.1.1 Natural bond orbital analysis

The mathematical description of the molecular wavefunction is usually given in terms of (canonical) molecular orbitals. In the natural bond orbital analysis these orbitals are transformed into various localized orbitals that more intuitively describe the chemical concepts of localized bonds and lone pairs than the original orbitals.[4]

The natural bond orbital analysis begins with an occupancy-weighted symmetric orthogonalization procedure. The orthogonalization procedure is a transformation from the original orbital basis to a set of orthonormal atom centered natural atomic orbitals (NAOs) that have an optimal occupancy for the species of interest.[8] The orthogonalization is required in order to avoid non-Hermitian terms in the Hamiltonian resulting from non-orthogonal atomic orbitals and the problems associated with the use of non-Hermitian Hamiltonians.[i] The occupancy weighting is used in the orthogonalization procedure to ensure that the forms of the orbitals with the highest occupancies are not significantly altered during the procedure.[8] The orbitals with low or no occupancy are then allowed to distort freely to meet the orthogonality requirements. The occupancy weighting guarantees that the orthogonalization procedure is stable and converges as the basis set is extended to completeness.

Other localized basis sets, for example, natural bond orbitals (NBOs) are derived from NAOs by using unitary transformations that maintain their orthogonality.[4] In order to obtain NBOs from NAOs the high occupancy (> 1.999 e) NAOs are first set as core orbitals. Then one-center orbitals whose occupancy exceeds a preset pair threshold (> 1.90 e) are assigned as lone-pair orbitals. Next two-center orbitals corresponding to (σ and π) bonds are sought. If an insufficient number of electron pairs is found, the search can be extended to three-center bonds. Furthermore, if the difference between the sum of occupancies in these orbitals and the total number of electrons exceeds one electron, the pair threshold is successively lowered (1.80,…,1.50) and the NBO search is repeated for each value. The set of orbitals corresponding to the highest sum occupancies is assigned as the "natural Lewis structure" and is generally found to agree with the bonds and lone pairs of the standard Lewis formula. The rest of the orbitals form the one-center Rydberg orbitals and the two- (or three-) center (σ^* and π^*) anti-bonds. The small occupancies of these anti-bonds correspond to the departures from the idealized Lewis picture and thus to small non-covalent corrections to the picture of localized covalent bonds.

2.1.2 Atoms in molecules theory

The theory of atoms in molecules (AIM) uses the topology of the total electron density distribution (calculated or experimental) of a molecule to derive information of bonding in the molecule.[6] The most striking features of electron density distributions are the local maxima that correspond to the core electrons of each atom. Atoms in the AIM theory are defined by assigning each local maximum of electron density a volume of the space (basin) that is delimited by zero flux surfaces. These unions of the local maxima and the corresponding basins provide a unique partitioning of the total electron

[i] Perturbation approaches, which are important tools for the calculation of properties of molecular systems, cannot be used together with non-Hermitian Hamiltonians because they can lead to a non-conservation of probability densities, complex energies, complex transition probabilities or other mathematical or physical inconsistencies.[4]

density. Integration of the electron density $\rho(\mathbf{r})$ over the basins yields atomic populations and thus atomic charges.

A chemical bond between two atoms is determined in the AIM theory by a ridge of maximum electron density called a bond path that links the bonded nuclei.[6] The electron density along the bond path has its minimum at the point where the bond path intersects the zero flux surface between the two atoms. This point is called a bond critical point (BCP). The properties of the electron density distribution at the BCPs are used to define the properties of the bonds that join atoms. In some structures, other types of critical points of the electron density are also found: ring critical points are a characteristic of ring structures and cage critical points are produced inside cages. The Poincarè–Hopf relation in a molecule and the Morse equation in a crystal determine the total number and type of non-degenerate critical points.[9]

The bond paths and the local maxima of the electron density define a chemical structure.[6] Although a bond path itself does not contain information of the number of electrons associated with the bond, the electron density at the BCP (ρ_{BCP}) can be related to the bond order through a comparison with bonds in a homogeneous series.

In addition to the electron density itself, another important source of information is the Laplacian of the electron density $\nabla^2\rho(\mathbf{r})$, which enhances the features of the electron density.[6] Positive values of the Laplacian [$\nabla^2\rho(\mathbf{r}) > 0$] correspond to local depletions of charge and negative values [$\nabla^2\rho(\mathbf{r}) < 0$] to local concentrations of charge. Empirically it has been found for compounds of lighter elements (≤ 2nd row) that these local concentrations of electronic charge closely map the localized electron domains assumed to be present in the valence shell of the central atoms in the VSEPR model.[10] The Laplacian thus provides a physical connection to the VSEPR model. The Laplacian values at BCPs have been used to define the nature of the bonds. For lighter elements negative values [$\nabla^2\rho(\mathbf{r}_{BCP}) < 0$] indicate covalent interactions between atoms and positive values [$\nabla^2\rho(\mathbf{r}_{BCP}) > 0$] either ionic or other types of closed shell interactions.[11] In contrast, the correspondence of the sign of the Laplacian at BCP with the nature of the bond has been shown to fail for heavier elements (fourth row and below).[9] Another measure called total energy density $H(\mathbf{r})$ has been suggested as a remedy.[12] The total energy density is the sum of kinetic energy density $G(\mathbf{r})$ (everywhere positive) and potential energy density $V(\mathbf{r})$ (everywhere negative). For covalent bonds, the $H(\mathbf{r})$ is negative at BCP and for closed shell interactions, it is positive at BCP. This has been shown to hold even for heavy elements.[9]

Localization $\lambda(A)$ and delocalization $\delta(A,B)$ indices have been defined in the framework of the AIM theory in order to have measures that are more

closely related to electron pairs and bond orders.[13,14,ii] A localization index gives the average number of electron pairs that are localized inside an atomic basin, and a delocalization index depicts the average number of electron pairs that are shared between two atoms.

At HF level of theory the $\delta(A,B)$ values have been shown to be in good agreement with the Lewis theory for nonpolar covalent bonds.[14] For polar bonds the $\delta(A,B)$ values tend to be smaller than the expected bond orders due to reduced covalency and for ionic bonds the $\delta(A,B)$ values are very small. Consequently a $\delta(A,B) < 1$ does not necessarily mean that the bonding results from the sharing of less than an electron pair, but rather that the electron pair is not equally shared. In a polyatomic molecule the $\delta(A,B)$ values tend to be somewhat less than one for equally shared pairs of electrons, due to the fact that the electrons on atoms A and B are also delocalized over other atoms in the molecule. In any case the delocalization index provides a practical measure of the covalent bonding between atoms.

2.1.3 Comparison of NBO and AIM methods

Although in this thesis the NBO and AIM theories are used as standards for the description of bonding, the bonding picture given by these two methods is not always consistent. The discrepancies in the bonding descriptions between the two methods arise from the different definitions they have for bonds orders and atomic charges.

The atomic charges calculated with the AIM method for polar bonds are usually larger than those calculated with the NBO or other methods.[15] On the other hand, trends of the atomic charges between different molecules produced by both methods agree in most cases. Therefore it is not recommended to compare atomic charges calculated with different methods or put too much weight on a single calculated atomic charge. It is more useful to determine how the calculated atomic charges of the species of interest compare to the atomic charges of other chemical species.

There can also be large discrepancies in the bond orders produced by the NBO and AIM methods. One of the most controversial examples of calculated bond orders are the homoatomic multiple bonds between the heavier ($n \geq 3$) main group elements.[16] The wavefunction analysis methods tend to predict bond orders that approach a triple bond for some of the heavy-atom acetylene

---

[ii] The pairing of electrons is a consequence of the Pauli Exclusion Principle.[14] Spatial localization of electron pairs is indirectly determined by the localization of the Fermi hole density. The Fermi hole density gives the extent of exclusion of other same spin electrons in the neighborhood of a reference electron. For a closed shell molecule the average number of electron pairs in the atomic basin of A and that in common between A and B are: $D_2(A,A) = \int_A d\mathbf{r}_1 \int_A d\mathbf{r}_2 \rho(\mathbf{r}_1,\mathbf{r}_2) = [N(A)^2 + F(A,A)]/2$; $D_2(A,B) = \int_A d\mathbf{r}_1 \int_B d\mathbf{r}_2 \rho(\mathbf{r}_1,\mathbf{r}_2) = [N(A)N(B) + F(A,B)]/2$, where $\rho(\mathbf{r}_1,\mathbf{r}_2)$ is the pair distribution function, $N(A)$ is the total electron density integrated over the atomic basin A and $F(A,A)$ and $F(A,B)$ are the total Fermi correlation contained within an atomic basin or shared between two basins, respectively. At HF level $F(A,A)$ and $F(A,B)$ are written in terms of the overlap integrals $S_{ij}(A)$ of the occupied orbitals over atomic basins: $F(A,A) = -\Sigma_i\Sigma_j S_{ij}(A)^2$ and $F(A,B) = -\Sigma_i\Sigma_j S_{ij}(A)S_{ij}(B)$. The localization index is defined as $\lambda(A) = F(A,A)$ and the delocalization index is defined as $\delta(A,B) = F(A,B) + F(B,A) = 2 \times F(A,B)$.

analogs with trans-bent geometries,[17,18] while the AIM method gives considerably lower bond orders for the same structures.[19] The differences between the methods arise from the fact that none of them actually measures the bond order but rather something else associated with the bond order. The bond order itself is not a measurable quantity but a chemical concept used to explain the observed structures. The higher bond orders predicted by wavefunction analysis for the heavy-atom analogs of acetylene reflect the way the bond orders are defined by these methods to account for the number of different electron pairs that take part in bonding, regardless of how strong their actual contribution is.[17] The AIM method on the other hand accounts only for the actual electron density (i.e. the number of electrons) that contributes to the bonding.[19] The wavefunction partitioning methods can be seen to give qualitative information about the mechanism of the bonding, whereas the AIM results are more related to the strengths of the bonds. As was the case with atomic charges, it is more useful for a chemical understanding to figure out the reasons for the calculated bond orders and not to concentrate too much on the absolute values of calculated bond orders.

2.2 Density functional calculations

The density functional theory (DFT) provides an attractive and efficient alternative to wavefunction methods for doing molecular calculations.[20] The premise behind DFT calculations is the theorem proven by Hohenberg and Kohn that there exists a functional $F[\rho(r)]$ of the electron density $\rho(r)$ of a system that uniquely determines the ground-state electronic energy of the system.[21] Using electron densities instead of wavefunctions to calculate the properties of electronic systems is advantageous because electron densities depend only on the three spatial coordinates while electronic wavefunctions depend on the coordinates of the electrons and become more complex as the number of electrons increases. In principle the knowledge of the exact density functional $F[\rho(r)]$ of an electronic system would give the total (non-relativistic) correlated energy of the system exactly with a computational effort comparable to HF calculations that lack the computationally difficult electron correlation.[22] Unfortunately the form of the exact functional $F[\rho(r)]$ is not known. Due to the elusiveness of the exact density functionals various approximate functionals have been developed.

In 1965 Kohn and Sham [23] suggested a formalism for developing new approximate density functionals, where all that can be calculated exactly is determined and the rest is summed up to a term called the exchange-correlation energy. In particular the exchange-correlation energy includes the non-classical contribution to the electron-electron interaction and the difference between the true kinetic energy of a system and that calculated for a non-interacting reference system.[20] Approximations for the exchange-correlation energy have been developed by parameterizing functions to best reproduce experimental results or by deriving expressions from quantum mechanics.[24] The modern

approximate density functionals are able to recover a substantial part of the total electron correlation.

Density functionals have been divided into different classes according to the way they represent the exchange-correlation energy.[20,24] The simplest density functional is the Xα method developed by Slater.[25] The Xα calculations include electron exchange but not their correlation and the accuracy of the results is usually similar to that of the HF calculations. The simplest approximation to include both electronic exchange and correlation is, one based only on electron density, called local density approximation (LDA).[20] LDA calculations have been successfully used in band structure calculations, but their performance in molecular calculations is not very good.[24] One of the failures of LDA calculations is that they tend to predict too short and strong bonds.[22] A further improvement of the theory uses both the electron density and its gradient.[20] This approximation is called generalized gradient approximation (GGA). In addition to these "pure" density functionals there are also hybrid methods that combine density functionals with parts of an HF calculation.[24] The current hybrid functionals give the most accurate results, although the performance of the GGA functionals is close to, and in some applications surpasses, that of the hybrid functionals. Compared to wavefunction based methods, GGA and hybrid functional calculations often give geometries and vibrational frequencies for stable molecules that are of comparable or better quality than those given by MP2 calculations.[22] However, there are some applications where density functionals do not work very well. One example is the failure of commonly used functionals to properly describe the weak interactions due to dispersion (van der Waals type interactions). Several approaches have been suggested to improve the description of weak interactions by DFT calculations,[26] but none of these methods have yet reached general acceptance.

In addition to commonly used GGA and hybrid functionals, functionals that go beyond the GGA approximation have been developed in recent years. These functionals belong to a group called meta-GGA functionals and they incorporate electronic kinetic energy density and second order gradients in the determination of the exchange-correlation energy.[27] Hybrid versions of the meta-GGA functionals have also been derived.[28] The latest development in hybrid functionals includes new double hybrid functionals, which add a non-local correction to correlation energy by using perturbation theory.[29] The perturbation approach makes the double-hybrid functionals computationally heavier than normal hybrid functionals. The use of these new functionals is not yet widespread but their performance compared to more conventional functionals has been encouraging.[29,30]

In this thesis the hybrid version of the functional by Perdew, Burke and Ernzerhof (PBE0) [31,32] has been the principal DFT method used in the calculations. Some of the early calculations were also done with the B3PW91 [33] and the MPW1PW91 [34] hybrid functionals. A revised version of the Perdew,

Burke and Ernzerhof GGA (rPBE) functional [31,35] was used in relativistic NMR shielding calculations.

2.3 Experimental structures of sulfur and selenium iodine cations

2.3.1 The nonexistence of neutral sulfur and selenium iodine species in the solid state under ambient conditions

Solid S_2I_2 has been made at the low temperature of 183 K by reacting HI/N_2 with a 0.1 mol dm^{-3} solution of S_2Cl_2 in pentane yielding a reddish-brown solid (S_8, I_2, and Cl_2 are also formed).[36] The characterization was based on an IR spectrum of the product that was shown to include bands corresponding to the stretching modes of S_2I_2 [ν(S-S) 510 cm^{-1}, ν_s(S-I) 295 cm^{-1}, ν_{as}(S-I) 305 cm^{-1}]. SI_2 has been identified by IR spectroscopy [ν_s(S-I) 368 cm^{-1}, ν_{as}(S-I) 376 cm^{-1}] in a matrix-isolation experiment as a product of a reaction between SCl_2 and I_2 at 9 K.[37] Both S_2I_2 and SI_2 decompose upon heating. The existence of SeI_2 and Se_2I_2 in a CS_2 solution (294 K) has been inferred from spectroscopic evidence,[38] but no binary selenium iodides have been isolated up to date. In general, neutral binary iodides of sulfur or selenium that are stable at ambient conditions are unknown.[2]

The instability of neutral binary sulfur and selenium iodides is attributed to a very low ionic resonance stabilization of the S-I and Se-I bonds.[2] The low ionic resonance stabilization is due to the similarity of the electronegativities of iodine (χ_I = 2.66), sulfur (χ_S = 2.58), and selenium (χ_{Se} = 2.55).[39] The S-I and Se-I bonds are even more unstable in the solid state due (in part) to the large sublimation energy of solid I_2 (62.3 kJ mol^{-1}). $SI_2(s)$ and $SeI_2(s)$ have been estimated to be unstable with respect to the elements according to reactions (1) and (2).[40]

$$(1/8)S_8(s) + I_2(s) \rightarrow SI_2(s) \qquad \Delta H = 32 \text{ kJ mol}^{-1} \qquad (1)$$

$$Se(\text{hexagonal}) + I_2(s) \rightarrow SeI_2(s) \qquad \Delta H = 13 \text{ kJ mol}^{-1} \qquad (2)$$

Sulfur and selenium iodine bonds have been successfully stabilized by adding large bulky ligands to the chalcogen atom. 4-tert-butyl-2,6-bis[(2,2'',6,6''-tetramethyl-m-terphenyl-2'-yl)methyl]phenyl sulfenyl iodide [41] and 2,4,6-tris-tert-butylphenyl selenenyl iodide [42] are examples of compounds with neutral sulfur and selenium iodine bonds. A similar kinetic stabilization technique has been used to stabilize reactive homoatomic multiple bonds of the heavier ($n \geq 3$) main group elements. A good example of the successful use of large bulky groups to stabilize homoatomic multiple bonds is the compound prepared by Sekiguchi et al.,[18] where a Si≡Si triple bond is stabilized by two large $[(Me_3Si)_2CH]_2(^iPr)Si$ groups.

Bulky ligands are not the only way to stable species with sulfur or selenium iodine bonds. In contrast to neutral species, the stabilization provided by crystal lattice energy affords the formation of stable ionic sulfur iodine and selenium iodine species in the solid state. SeI_6^{2-} was the first known structure

with stable covalent bonds between iodine and selenium.[43] Since the 1970's Passmore et al.[2] have prepared and characterized a number of species with sulfur and selenium iodine cations. The structures and bonding of these interesting cations will be reviewed in the following sections.

2.3.2 $(SeI_3)[MF_6]$ (M = As, Sb)

The simplest selenium iodine cation that has been characterized in solid state by X-ray crystallography is the pyramidal SeI_3^+.[44] $(SeI_3)[MF_6]$ (M = As, Sb) [44,45] has been prepared according to reactions (3) and (4).

$$2Se + 3I_2 + 3AsF_5 \xrightarrow{SO_2(l)} 2(SeI_3)[AsF_6] + AsF_3 \quad (3)$$

$$6Se + 9I_2 + 10SbF_5 \xrightarrow{SO_2(l)} 6(SeI_3)[SbF_6] + (SbF_3)_3{\cdot}SbF_5 \quad (4)$$

$(SeI_3)[AsF_6]$ forms small black crystals and $(SeI_3)[SbF_6]$ brown-black crystals.[45] Both compounds are stable at room temperature when stored under dry nitrogen although $(SeI_3)[AsF_6]$ was reported to be unstable towards light and X-rays.[44,45]

The SeI_3^+ cation is of approximately C_{3v} symmetry and it can be regarded as having AX_3E tetrahedral geometry in terms of VSEPR theory with the lone pair of electrons occupying one of the vertices.[45] The average experimental Se-I distance is 2.510 Å and the I-Se-I angle is 102.4°.

The FT-Raman spectrum of $(SeI_3)[AsF_6]$ was reported and assigned in the original research paper **III**.

2.3.3 $(S_2I_4)[MF_6]_2$ (M = As, Sb)

Several attempts have been made to prepare the sulfur analogue of SeI_3^+ without any success.[46] A number of reactions designed to give $(SI_3)[AsF_6](s)$ have all led to the formation of $(S_2I_4)[AsF_6]_2(s)$ and $I_2(s)$. $S_2I_4^{2+}$ seems to be the simplest sulfur iodine cation that can be isolated in the solid state.

$(S_2I_4)[MF_6]_2(s)$ (M = As, Sb) has been quantitatively prepared according to reactions (5) and (6).[46]

$$(1/4)S_8 + 2I_2 + 3AsF_5 \xrightarrow{SO_2(l)} (S_2I_4)[AsF_6]_2 + AsF_3 \quad (5)$$

$$(5/4)S_8 + 10I_2 + 18SbF_5 \xrightarrow{SO_2(l)} 5(S_2I_4)[SbF_6]_2 + 5SbF_3{\cdot}3SbF_5 \quad (6)$$

$S_2I_4^{2+}$ has a distorted right triangular prism structure in both MF_6^- salts.[46] The structure of $S_2I_4^{2+}$ is significantly different from the structure of the isoelectronic P_2I_4 (see Figure 1),[47] which has the structure predicted by the VSEPR theory and the Lewis bonding model. The $S_2I_4^{2+}$ cations have the shortest S-S bond lengths so far reported for an isolated compound: 1.818(10) Å (SbF_6^-) and 1.843(6) Å (AsF_6^-), corresponding to Pauling bond orders of 2.7 and 2.4, respectively.[1,46] The I-I bond distances 2.571 Å (SbF_6^-) and 2.599 Å (AsF_6^-) are also relatively short, corresponding to Pauling bond orders of 1.4 and 1.3. In contrast the S-I bond distances of 2.993(4) Å (SbF_6^-) and 3.019 Å (average) (AsF_6^-) are very long and comparable to the sulfur iodine distances in sulfur

iodine charge transfer complexes [e.g. the S-I bond in $C_7H_6O_4S_3 \cdot I_2$ 2.9122(13) Å [48] and in $C_7H_5NOS \cdot 2I_2$ 2.874(2) Å].[49]

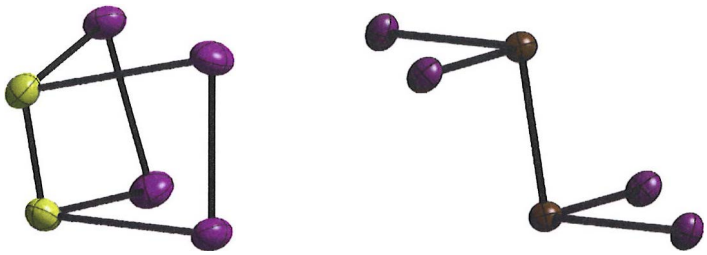

Figure 1. The structures of the $S_2I_4^{2+}$ cation in $(S_2I_4)[AsF_6]_2$ [1] (left) and P_2I_4 molecule [47] (right).

The structure of $S_2I_4^{2+}$ has been described as consisting of $S_2^{0.66+}$ and two $I_2^{0.66+}$ units weakly joined by so-called π*- π* bonds.[46] These bonds are formed when the electrons in the two mutually perpendicular π* orbitals of $S_2(^3\Sigma_g^-)$ interact with the lone electrons in the π* orbitals of each I_2^+.The interaction results in two mutually perpendicular four-center two-electron π*- π* bonds that are shown in Figure 2. Following the bond formation, the positive charge is expected to delocalize over the entire cation as a consequence of the near equality of the ionization energies of I_2 (9.39 eV) and S_2 (9.40 eV).

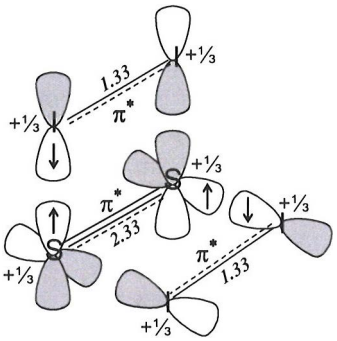

Figure 2. According to the simple bond model, the π*- π* bonds of $S_2I_4^{2+}$ and the positive charge delocalization result in an equal charge distribution over all atoms in the cations and S-S and I-I bond orders of 2.33 and 1.33, respectively.

It has been proposed that $S_2I_4^{2+}$ and related species adopt their π bonded structures instead of the more common σ bonded alternatives because the positive charge is much more delocalized in the π bonded structures.[46] The positive charge is thought to be formally localized on adjacent sulfur atoms in

the σ bonded alternative of $S_2I_4^{2+}$, causing the energy of the cation to rise due to increased coulomb repulsion.

2.3.4 $(Se_2I_4)[Sb_2F_{11}]_2$ and $(Se_2I_4)[AsF_6]_2{\cdot}SO_2$

$(Se_2I_4)[Sb_2F_{11}]_2$ [50] and $(Se_2I_4)[AsF_6]_2{\cdot}SO_2$ [51] have been quantitatively prepared by reactions (7) and (8), respectively.

$$2Se + 2(I_2)[Sb_2F_{11}] \xrightarrow{SO_2(l)} (Se_2I_4)[Sb_2F_{11}]_2 \qquad (7)$$

$$2Se + 2I_2 + 3AsF_5 \xrightarrow{SO_2(l)} (Se_2I_4)[AsF_6]_2{\cdot}SO_2 + AsF_3 \qquad (8)$$

In both salts, $Se_2I_4^{2+}$ has very similar eclipsed geometries that are distinctly different from the structure of $S_2I_4^{2+}$.[51] Although both $S_2I_4^{2+}$ and $Se_2I_4^{2+}$ can be described as having distorted trigonal prismatic structures, $Se_2I_4^{2+}$ differs from $S_2I_4^{2+}$ by having a long chalcogen-chalcogen bond distance. The Se-Se distance in $Se_2I_4^{2+}$ is 2.841(6) Å (AsF_6^- salt)[51] [cf. α-Se_8 2.336(6) Å].[52] The Se-I bonds in $Se_2I_4^{2+}$ (average 2.451 Å)[51] are shorter than those in SeI_3^+ (average 2.510 Å)[45] and that in 2,4,6-$tBu_3C_6H_2Se$-I (2.529 Å).[42] The *syn* iodine interactions (average 3.673 Å) are shorter than twice the sum of van der Waals radii of iodine (4.30 Å),[39] but longer than the iodine-iodine contacts between I_2^+ units in I_4^{2+} [3.270(1) Å (AsF_6^- salt)][53] and I_5^+ cations in I_{15}^{3+} [3.416(3) Å (SbF_6^- salt)].[54] The overall geometry of $Se_2I_4^{2+}$ is similar to the geometry of $S_2O_4^{2-}$.[55]

$Se_2I_4^{2+}$ has been described as a weak dimer of two SeI_2^+ radical cations (see Figure 3).[51] The Se-I bonds have formal bond orders of 1¼ consistent with the removal of one electron from the π* anti-bonding HOMO of each SeI_2. The weak bonding between SeI_2^+ units has been suggested to arise from the interaction of the SOMOs of SeI_2^+, which forms a delocalized six-center two-electron π*- π* bond between the SeI_2^+ units. This π*- π* bond effectively delocalizes the positive charge over the cation and makes the cluster-like structure of $Se_2I_4^{2+}$ more stable than the all σ bonded *trans* alternative predicted by the VSEPR theory would be.

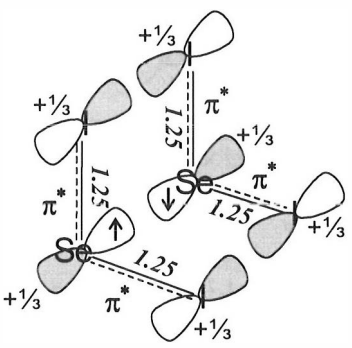

Figure 3. The simple bond model describes $Se_2I_4^{2+}$ as a π*- π* bonded dimer of two SeI_2^+ radical cations.

The reason for the different bonding in $S_2I_4^{2+}$ and $Se_2I_4^{2+}$ structures has been attributed to the higher energy of the S-S π bond (199 kJ mol^{-1}) compared to the Se-Se π bond (100 kJ mol^{-1}) and the near equality of the first ionization energies of S_2 (9.40 eV) and I_2 (9.39 eV) compared to Se_2 (8.90 eV).[51] The higher π bond energy of sulfur is expected to favor the S-S π bond formation over the S-I σ bond formation. Furthermore the similarity of the S_2 and I_2 ionization energies is thought to significantly facilitate the multicenter bond formation between S_2 and I_2 compared to what it would be between Se_2 and I_2.

2.3.5 $(Se_6I_2)[AsF_6]_2{\cdot}2SO_2$

Dark red crystals of $(Se_6I_2)[AsF_6]_2{\cdot}2SO_2$ have been prepared with two different reaction routes (9) and (10).[56,57]

$$6Se + I_2 + 3AsF_5 \xrightarrow{SO_2(l)} (Se_6I_2)[AsF_6]_2{\cdot}2SO_2 + AsF_3 \quad (9)$$

$$2(Se_8)[AsF_6]_2 + 2(SeI_3)[AsF_6] \xrightarrow{SO_2(l)} 3(Se_6I_2)[AsF_6]_2{\cdot}2SO_2 \quad (10)$$

$(Se_6I_2)[AsF_6]_2{\cdot}2SO_2$ is stable at 253 K under dry nitrogen but attempts to remove the solvent molecules have been reported to be unsuccessful, resulting in decomposition of $(Se_6I_2)[AsF_6]_2{\cdot}2SO_2$.[57]

The structure of $Se_6I_2^{2+}$ contains a hexaselenium ring in a chair conformation substituted by two iodine atoms in the 1,4-positions with *endo* orientations, which gives the cation a distorted cube-like shape (see Figure 4).[57] The Se-I bond lengths [2.454(2) Å] are notably shorter than in SeI_3^+ (average 2.510 Å)[45] and similar to those in $Se_2I_4^{2+}$ (average 2.451 Å).[51] The Se(tricoordinate)-Se(dicoordinate) bonds (average 2.475 Å) are considerably longer than the adjacent Se(dicoordinate)-Se(dicoordinate) bonds [2.227(2) Å]. This bond alternation has been suggested to result from the delocalization of the positive charge from the tricoordinate selenium atoms to other selenium atoms in the ring. The relatively short Se-I bonds have also been related to the delocalization of the positive charge from the ring to iodine atoms.

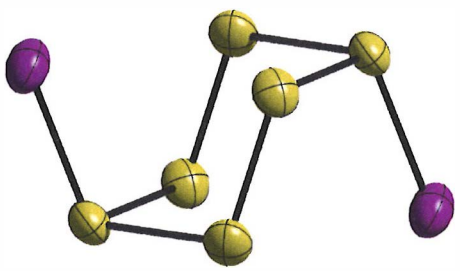

Figure 4. The structure of the $Se_6I_2^{2+}$ cation in $(Se_6I_2)[AsF_6]_2{\cdot}2SO_2$.[56]

The mechanism suggested for the charge delocalization assumes that there is some donation of electron density from the Se-I π* orbital to the partially positively charged dicoordinate selenium atoms.[57] This donation leads to a

reduction of the π^* electron density in the exocyclic Se-I bond, decreases its bond length and results in a partial positive charge on the iodine atom. It is also suggested to lead to the formation of weak bonding interactions between the iodine atoms and the dicoordinate selenium atoms (average distance 3.714 Å cf. the sum of selenium and iodine van der Waals radii 4.15 Å),[39] which could explain why $Se_6I_2^{2+}$ adopts a cube-like shape and not the less sterically hindered isomer, where the iodine atoms would be in *exo* positions with respect to the ring.

The delocalization of positive charge over all eight atoms and the observed trends in the bond lengths have been rationalized in the literature by a resonance between five valence structures as shown in Figure 5.[58] Valence structure **i** represents the "parent" Lewis structure where the positive charges are localized on the tricoordinate selenium atoms. Valence structures **ii** and **iii** show the delocalization to other selenium atoms in the ring and **iv** and **v** the delocalization to iodine atoms.

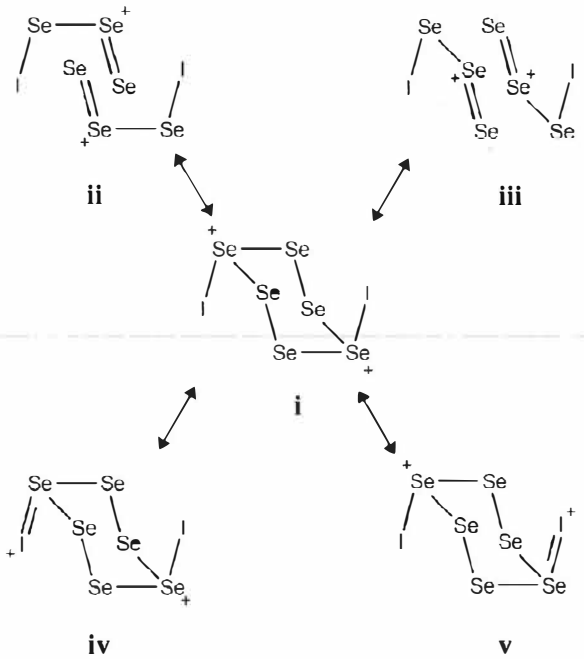

Figure 5. Valence structure description of the bonding of $Se_6I_2^{2+}$.

2.3.6 $(Se_6I)_n \cdot nMF_6$ (M = As, Sb)

$(Se_6I)_n \cdot n[AsF_6]$ has been reported to form relatively large crystals (ca. 2.0 × 1.0 × 0.25 mm) that appear golden in reflected light and deep ruby red in transmitted light.[59] The crystals of $(Se_6I)_n \cdot n[SbF_6]$ are small in size but the physical appearance has been reported to be otherwise similar to $(Se_6I)_n \cdot n[AsF_6]$ in both reflected light (golden) and transmitted light (ruby red).[57] Both $(Se_6I)_n \cdot n[MF_6]$ (M = As, Sb) are stable at room temperature under dry nitrogen.

The stoichiometric preparation of $(Se_6I)_n{\cdot}n[AsF_6]$ has been carried out according to reaction (11). The crystals of $(Se_6I)_n{\cdot}n[SbF_6]$ have been prepared by reaction between selenium and $(I_2)[Sb_2F_{11}]$, but the reaction was reported to be complex and all the products have not been identified.

$$12Se + I_2 + 3AsF_5 \xrightarrow[11\ days]{SO_2(l),\ room\ temp} (2/n)(Se_6I)_n{\cdot}n[AsF_6] + AsF_3 \qquad (11)$$

Both $(Se_6I)_n{\cdot}n[MF_6]$ (M = As, Sb) salts contain polymeric strands of $(Se_6I^+)_n$.[57] The polymeric strands are formed of Se_6 rings that are linked with bridging iodine atoms. The Se_6 rings have chair conformations and the iodine atoms are bound to the 1,4 positions in an *endo* configuration, giving the ISe_6I units within the $(Se_6I^+)_n$ strands a similar appearance to that of $Se_6I_2^{2+}$.

There is some Se-Se bond alternation within the Se_6 rings [average Se(tricoordinate)-Se(dicoordinate) 2.366 Å and average Se(dicoordinate)-Se(dicoordinate) 2.294 Å], but it is less pronounced than that in $Se_6I_2^{2+}$ in line with the lower positive charge per hexaselenium ring in $(Se_6I^+)_n$.[57] The bridging Se-I bonds [average 2.739 Å] are much longer than those in SeI_3^+ but similar to those in $C_4H_8OSe{\cdot}I_2$ [2.755(4) Å],[60] which contains an Se-I bond with a formal bond order of 0.5. The linear bonding arrangement around the bridging iodine atoms can, therefore, be regarded as a three-center two-electron Se-I-Se bond.

All attempts to prepare AsF_6^- salts of selenium iodine cations with a higher selenium content have led to either $(Se_6I_2)[AsF_6]_2{\cdot}2SO_2$ or $(Se_6I)_n{\cdot}nAsF_6$ in the solid state.[57]

2.3.7 $(S_7I)[MF_6]$ (M = As, Sb)

$(S_7I)[MF_6]$ (M = As, Sb) was the first stable binary sulfur iodine cation characterized.[61] The S_7I^+ cation has been prepared with a variety of different routes and it can be made for example by reacting excess of sulfur and iodine with arsenic or antimony pentafluoride in liquid SO_2 according to equations (12) and (13).[62]

$$7S_8 + 4I_2 + 12AsF_5 \xrightarrow{SO_2(l)} 8(S_7I)[AsF_6] + 4AsF_3 \qquad (12)$$

$$21S_8 + 12I_2 + 40SbF_5 \xrightarrow{SO_2(l)} 24(S_7I)[SbF_6] + 4(SbF_3)_3[SbF_5] \qquad (13)$$

$(S_7I)[AsF_6]$ has been reported to form orange-brown crystals and $(S_7I)[SbF_6]$ large shiny brown-black crystals that appear to be translucent red-orange when freshly cut.[62] Solid $(S_7I)[AsF_6]$ decomposes slowly (several weeks) at room temperature whereas $(S_7I)[SbF_6]$ is reported to be stable in the same conditions. Both $(S_7I)[MF_6]$ (M = As, Sb) are stable at 253 K. In addition to $(S_7I)[MF_6]$ (M = As, Sb), the S_7I^+ cation has been found in the $(S_7I)_4(S_4)[AsF_6]_6$ salt.[63]

The crystal structure of S_7I^+ presented in Figure 6 has a seven-membered sulfur ring in a slightly distorted chair conformation similar to those found in γ- and δ-Se_7,[64] and an exocyclic iodine atom.[62] The overall geometry of S_7I^+ is similar to that of S_7O.[65] The sulfur ring exhibits a similar bond length alternation

as that observed in the selenium ring of $Se_6I_2^{2+}$.[57] The S-S bonds from the tricoordinate sulfur atom are considerably longer than the other bonds in the ring. The adjacent bonds are relatively short and from there on the bond length alternation continues around the ring. A part of the bond alternation has been attributed to the bond alternation intrinsic to S_7, and the rest has been suggested to be due to the delocalization of the positive charge from the tricoordinate sulfur atom to the ring. The position of the substituted iodine atom is such that the delocalization of charge from the tricoordinate sulfur enhances maximally the bond alternation in the S_7 ring. The S-I bond [2.342(3) Å] is shorter than the S-I single bond in a neutral compound [cf. S-I bond 2.406(4) Å in $(Ph)_3CSI$],[66] which infers that some of the positive charge could be delocalized to the iodine atom analogously to $Se_6I_2^{2+}$. Judging by the S-I distances the iodine atom also has a weak bonding interaction with another sulfur atom located at the base of the S_7 ring [3.394(3) Å, cf. the sum of sulfur and iodine van der Waals radii 4.00 Å].[39]

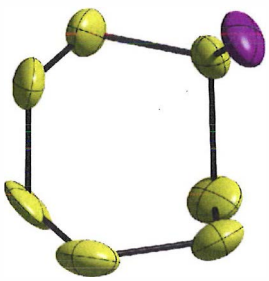

Figure 6. The structure of S_7I^+ cation in $(S_7I)[AsF_6]$.[62]

2.3.8 $[(S_7I)_2I][SbF_6]_3 \cdot 2AsF_3$

The largest binary sulfur iodine cation characterized so far is $(S_7I)_2I^{3+}$.[67] Its salt $[(S_7I)_2I][SbF_6]_3 \cdot 2AsF_3$ has been prepared by reaction (14).

$$7S_8 + 6I_2 + 20SbF_5 \xrightarrow{AsF_3(l)} 4[(S_7I)_2I][SbF_6]_3 \cdot 2AsF_3 + 2(SbF_3)_3[SbF_5] \quad (14)$$

$(S_7I)_2I^{3+}$ has two S_7I^+ cations joined via a bridging iodine atom located at an inversion centre (see Figure 7).[67] The configuration of S_7I^+ units is the same in $(S_7I)_2I^{3+}$ and in $(S_7I)[MF_6]$ (M = As, Sb) and the bond distances and bond angles within the rings are similar.[62] The S-I bonds from the bridging iodine atom have a linear arrangement and a bond distance of 2.674(7) Å, which is similar to that of the linear S-I-S bond in the $[(H_2N)_2CS]_2I^+$ ion (2.629 Å).[68] The linear S-I-S bond can be regarded as a three-center two-electron bond and the bridging S-I bonds can be assigned formal bond orders of 0.5.

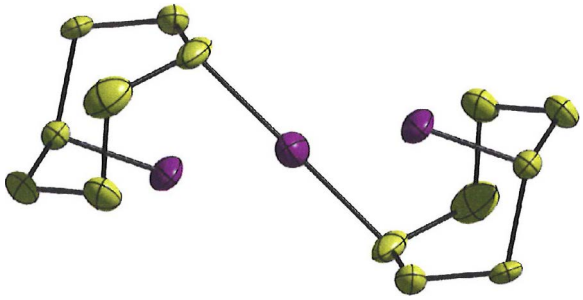

Figure 7. The structure of the $(S_7I)_2I^{3+}$ cation in $[(S_7I)_2I][SbF_6]_3 \cdot 2AsF_3$.[67]

2.4 Results and discussion

The following sections review the most important findings on bonding in articles **I**, **II** and **IV**.

2.4.1 The highly homoatomic $n_{p\pi}$ - $n_{p\pi}$ ($n \geq 3$) bonded $S_2I_4^{2+}$

The high experimentally determined homoatomic bond orders (see paper **I** for details) and the rather unusual cluster-like structure make $S_2I_4^{2+}$ an interesting subject for bonding studies. The π^*- π^* bond model (see Figure 2) that has been used to describe the bonding in $S_2I_4^{2+}$ was originally derived by Passmore et al. using simple frontier molecular orbital theory.[46] Some support for the proposed bonding model was presented through rudimentary HF/STO-3G calculations using $O_2Cl_4^{2+}$ as a model system.[46] However, the use of a π^*- π^* bond model for $S_2I_4^{2+}$ still lacked sound theoretical justification, and an investigation testing the simple bonding model against more rigid theoretical bonding models was warranted. The results of this theoretical study have been published in full length in paper **II**.

The optimization of a reasonable structure for $S_2I_4^{2+}$ proved to be a challenge. HF and correlated MP2 calculations did not yield stationary points corresponding to the observed experimental structures.[I] It required the use of hybrid DFT methods to obtain optimized structures in reasonable agreement with the crystal structures. Further support for the good performance of hybrid DFT methods in modeling the properties of $S_2I_4^{2+}$ was provided by a high level optimization using a correlated coupled cluster CCSD method that gave a structure very close to the DFT optimized structures, and by the good agreement between observed vibrational frequencies and those calculated at a hybrid DFT level. Following the good performance of hybrid DFT methods in modeling the properties of $S_2I_4^{2+}$, hybrid DFT methods were chosen as the principal method of calculation also in all other studies of this thesis.

An AIM analysis of $S_2I_4^{2+}$ confirmed that the weak bonds between sulfur and iodine atoms are real and all bonds in the cation are covalent in nature. These AIM results provided a basis for the successful use of any covalent bonding model, such as the π^*- π^* bond model, to describe the bonding in $S_2I_4^{2+}$. The bond orders predicted by the simple bonding model for S-S and I-I bonds

(see Figure 2) agreed well with the bond orders derived from MO, AIM and NBO analyses (S-S ~ 2.2 and I-I ~ 1.4) and with those calculated from experimental results. The delocalized 4c2e π^*- π^* bonds suggested by the simple bonding model to account for the bonding between sulfur and iodine atoms were also in agreement with the S-I bond orders (~ 0.3) predicted by MO, AIM, and NBO analyses, even though the simple bonding model did not directly provide an estimate for the S-I bond orders.

The calculated AIM and NBO atomic charges indicated that the equal distribution of the positive charge suggested by the simple bonding model oversimplifies the actual charge distribution; the positive charge is actually more localized on the iodine atoms than on the sulfur atoms. However, the calculated atomic charges also showed that the positive charge is more delocalized in the experimental structure of $S_2I_4^{2+}$ than in the calculated, approximately singly bonded *trans*-alternative.[iii] The calculated atomic charges confirmed the hypothesis that charge delocalization is one of the driving forces for $S_2I_4^{2+}$ to adopt the observed non-classical structure.

A comparison of the high S-S bond order of $S_2I_4^{2+}$ with other sulfur species led to the conclusion that $S_2I_4^{2+}$ exhibits the highest known S-S bond order in an isolated compound.[I,II] The S-S bond order was also compared to the highly debated Si-Si "triple bond" found by Sekiguchi et al.[18] in RSi≡SiR {R = Si(^{i}Pr)[CH(Me$_3$Si)$_2$]$_2$}.[69] The comparison was made in order to test whether the S-S bond would still be a contender for the title of the bond with the highest homoatomic bond order among the heavier (n ≥ 3) main group elements. A smaller $Si_2(SiH_3)_2$ molecule was used in the calculations to model the Si-Si "triple bond" in Sekiguchi's compound. The bond orders were found to depend heavily on the methods used to determine them. The S-S bond order was determined to be at best similar to, but in general lower than, the Si Si bond order, depending on the method used in the determination.

2.4.2 The Se-I π bonded $Se_2I_4^{2+}$

Compared to $S_2I_4^{2+}$, the structure of $Se_2I_4^{2+}$ exhibits a fundamentally different bonding even though their structures might look similar at first glance. Passmore et al. have described $Se_2I_4^{2+}$ as a weak dimer of two SeI_2^+ cations bound together by a 6c2e π^*- π^* bond (see Figure 3) based on a simple frontier molecular orbital treatment.[51] This bonding description was supported by HF/STO-3G [51] and VB/STO-5G [70] calculations using $S_2Cl_4^{2+}$ as a model system, but challenged later by another study describing $Se_2I_4^{2+}$ as a 10π aromatic system and the bonding between SeI_2^+ units with a 6c10e π bond.[71]

In the simple bonding model, the bonding of $Se_2I_4^{2+}$ is characterized by the HOMO presented in Figure 8 and contributions from lower MOs to the bonding are neglected. Analysis of MOs (see paper **II** for details) indicated that for a

---

[iii] This structure is analogous to the structure of P_2I_4 and was obtained via partial optimization by constraining the S-S bond to an approximate single bond length between positively charged sulfur atoms (2.124 Å).[II] No real minimum structure corresponding to P_2I_4 structure was found for $S_2I_4^{2+}$.

thorough description of the bonding of $Se_2I_4^{2+}$ all valence orbitals need to be included since also the lower orbitals have non-vanishing contributions to the intradimer bonding. Therefore both the 6c2e π*- π* bond and the 6c10e π bond pictures are only approximations of the total bonding. The choice between these pictures is first of all determined by how well they describe the properties of the system. Furthermore, simplicity is desired from bonding models because that makes them easier to apply to different species. The bond orders (e.g. Se-I 1¼) and the charge delocalization predicted by the 6c2e π*- π* bond model were already in good agreement with the bond orders and atomic charges obtained from AIM, NBO, and MO analyses. The 6c10e π bond description introduces the idea of describing $Se_2I_4^{2+}$ as a π aromatic system. However it remains unclear how defining $Se_2I_4^{2+}$ as an aromatic system improves the understanding of the properties of $Se_2I_4^{2+}$; the 6c2e π*- π* bond model is considered to be the better description of the bonding due to its simplicity. The simplicity of the π*- π* bond model makes it a useful tool for a qualitative description of the bonding in many species of the electron-rich elements. Examples to date include $(S_3N_2)_2^{2+}$,[72] $(XCNSSS)_2^{2+}$ (X = Cl, Br, I),[73] $(NSNSCCNSSN)_2^{2+}$,[74] O_8,[75] $O_2Cl_2^+$,[76] Te_6^{4+},[77] and $[TCNE]_2^{2-}$.[78]

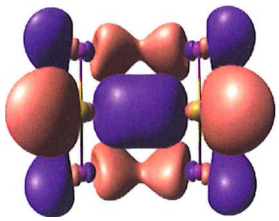

Figure 8. HOMO of $Se_2I_4^{2+}$ (isosurface 0.035).

2.4.3 Why do $S_2I_4^{2+}$ and $Se_2I_4^{2+}$ have different structures?

The relative stabilities of the calculated structures shown in Figure 9 favor the experimentally observed structures for both $S_2I_4^{2+}$ (**A** conformation) and $Se_2I_4^{2+}$ (**B** conformation). For $Se_2I_4^{2+}$ even the partially optimized, approximately singly bonded *trans*-structure is calculated to have lower energy than the **A** structure, where the bonding is similar to that of $S_2I_4^{2+}$.

Investigation of the energetic causes for the different minimum structures was conducted in Paper **II** by examining the steps of a Born-Haber cycle written for an isomerization reaction from **A** structure to **B** structure given in Figure 10. The step reactions were divided into three classes according to the type of processes they represented: **a)** breaking and forming of π*- π* bonds (reactions **i** and **viii**), **b)** ionization of E_2, X_2 and EX_2 molecules (reactions **ii**, **iii**, and **vii**) and **c)** breaking of strong dichalcogen and dihalogen bonds and forming of chalcogen-halogen bonds (reactions **iv**, **v** and **vi**). The sums of $\Delta_rH°$ in **a)** and **b)** type processes were shown to be similar for both $S_2I_4^{2+}$ and $Se_2I_4^{2+}$. The difference in the sums of $\Delta_rH°$ for the **c)** type processes accounted for almost all of the stability difference between the $S_2I_4^{2+}$ and $Se_2I_4^{2+}$ isomers.

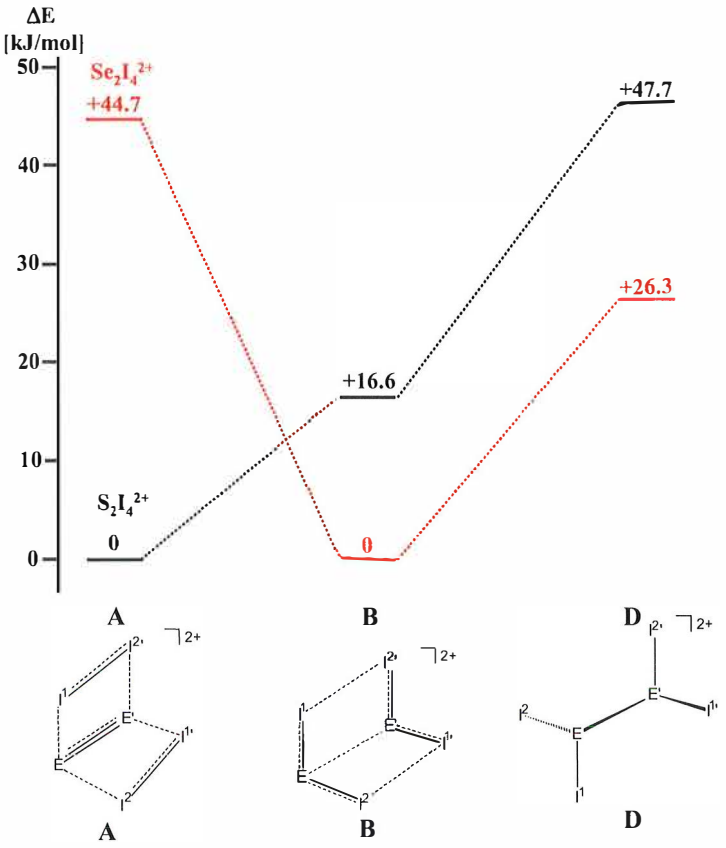

Figure 9. Relative stabilities of different conformations of $S_2I_4^{2+}$ and $Se_2I_4^{2+}$ calculated at CCSD(T)/(SDB)-cc-pVTZ//PBE0/(SDB)-cc-pVTZ level of theory.[II]

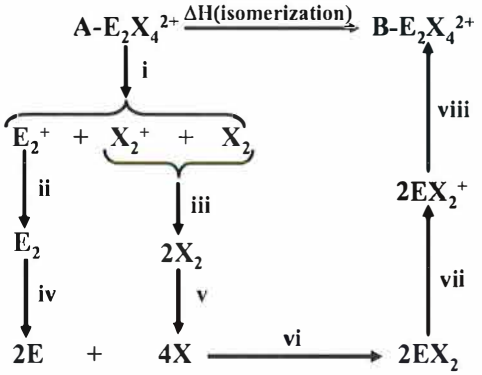

Figure 10. The Born-Haber cycle for the isomerization reaction from **A** structure to **B** structure.[II]

The different stabilities of homoatomic bonds compared to the chalcogen-iodine bonds were concluded to be the main causes for $S_2I_4^{2+}$ and $Se_2I_4^{2+}$ to adopt their different structures as indicated by the enthalpy difference of **c)** type processes. The previously proposed difference in the ionization energy of Se_2 compared to S_2 and I_2 seemed to play only a minor role. The calculated atomic charges also inferred that charge delocalization has a role in stabilizing the **A** structure of $S_2I_4^{2+}$ compared to the **B** structure, whereas for $Se_2I_4^{2+}$ the charge distribution remained relatively similar in both isomers.

A comparison of **A** and **B** structures for a group of related chalcogen-iodine cations ($I_2SeSI_2^{2+}$, $S_2Cl_4^{2+}$, $S_2Br_4^{2+}$ and $Te_2I_4^{2+}$) revealed that $S_2I_4^{2+}$ is the only one to exhibit the **A** structure. This underlines the extraordinary nature of $S_2I_4^{2+}$ that rises from the high strength of the S–S π bond compared to the S-I σ bond.

2.4.4 Why has SI_3^+ not been prepared?

As all attempts to prepare SI_3^+ have led to the formation of $S_2I_4^{2+}$, it was presumed that SI_3^+ might not be energetically stable towards $S_2I_4^{2+}$. In order to test the hypothesis the $\Delta_rH^\bullet$ for reactions (15)-(17) presented in Table 1 were estimated.

Table 1. Enthalpies of reactions $\Delta_rH°(298\ K)$ [kJ mol^{-1}] in different phases E = S, Se

		S	Se [a]
(15)	$2\ EI_3^+(g) \leftrightharpoons E_2I_4^{2+}(g) + I_2(g)$	+285	+341
(16)	$2\ (EI_3)[AsF_6](s) \leftrightharpoons (E_2I_4)[AsF_6]_2(s) + I_2(s)$	–287	–209 [b]
(17)	$2\ EI_3^+(SO_2) \leftrightharpoons E_2I_4^{2+}(SO_2) + I_2(SO_2)$	-5	+45

[a] Energies for selenium species have been calculated using the methods given in paper **I**. [b] Ion volumes for lattice enthalpy estimations have been adopted from references 45, 51, and 79.

As Expected $\Delta_rH°$ for the gas phase reaction (15) strongly favors the $SI_3^+(g)$ due to the higher positive charge on $S_2I_4^{2+}(g)$. However, since the actual compounds are solid salts, an estimation of the corresponding solid phase energetics is required. The enthalpy change for the solid state reaction (16) was estimated using the Born–Fajans–Haber cycle presented in Figure 11. Lattice enthalpies have been calculated from estimated volumes of the AsF_6^- salts according to a procedure given in paper **I**. Similar treatments have been successfully used to estimate the energetics of homopolyatomic cations of groups 16 and 17 and related salts in the solid state.[80,81]

The high lattice enthalpy of $(S_2I_4)[AsF_6]_2(s)$ (Δ_LH = 1432 kJ mol^{-1}) appears to be large enough compared to the lattice enthalpy of $(SI_3)[AsF_6](s)$ (Δ_LH = 461 kJ mol^{-1}) to compensate for the positive gas phase energy and make $(S_2I_4)[AsF_6]_2$ strongly favored in the solid state. $(S_2I_4)[AsF_6]_2(s)$ is concluded to be lattice stabilized towards the addition of I_2 and the formation of $(SI_3)[AsF_6](s)$. In a similar manner to the reaction (16), $(S_2I_4)[AsF_6]_2(s)$ was shown in paper **I** to be lattice stabilized towards dissociation into various other monocations.

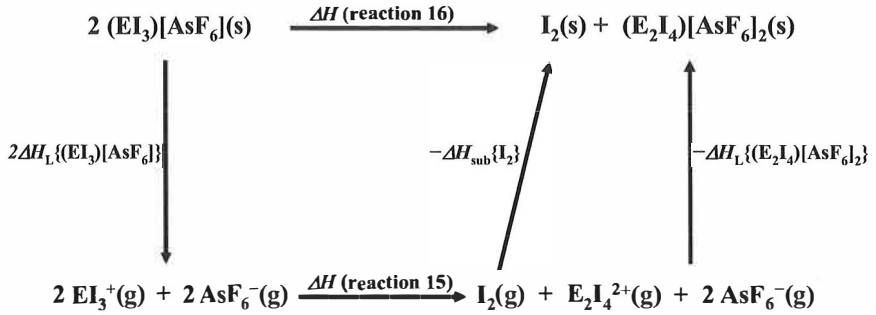

Figure 11. Born-Fajans-Haber cycle for the formation of $(EI_3)[AsF_6]$ (E = S, Se).

Following the reasoning for the sulfur reaction, the selenium reaction (16) is expected to have a reaction enthalpy that is either positive or at least close to zero owing to the fact that $(SeI_3)[AsF_6](s)$ has been successfully prepared. $\Delta_rH°$ for the gas phase reaction (15) is somewhat higher for selenium than for sulfur, but it is not nearly enough to compensate for the higher lattice energy of $(Se_2I_4)[AsF_6]_2(s)$ (Δ_LH = 1426 kJ mol^{-1}) and make $(SeI_3)[AsF_6](s)$ (Δ_LH = 469 kJ mol^{-1}) stable in the solid state. This result contradicts the conclusion that the fact of finding SeI_3^+ but not SI_3^+ is governed by the solid state energetics.

In order to further investigate the problem, reaction enthalpies in an SO_2 solution were calculated. The $\Delta_rH°$ of reaction (17) for the sulfur species is slightly endothermic, which could infer that the formation of SI_3^+ in an SO_2 solution is not favored. This point of view is supported by the fact that no peaks assignable to SI_3^+ were observed in the FT-Raman spectra of an SO_2 solution of $(S_2I_4)[AsF_6]_2$ and I_2.[1] In contrast to SI_3^+, SeI_3^+ appears to be favored over $Se_2I_4^{2+}$ in an SO_2 solution, if enough I_2 is present. The calculation result is in agreement with a ^{77}Se NMR spectrum (−70 °C) measured for a mixture of $(Se_2I_4)[AsF_6]_2$ and I_2, which showed only one peak at 834 ppm that was assigned to SeI_3^+.[51] In conclusion, the calculated reaction enthalpies indicate that the success in preparing SeI_3^+ but not SI_3^+ is most likely due to their different stabilities in an SO_2 solution and not due to the solid state energetics.

2.4.5 Bond alternation in 1,4-$Se_6I_2^{2+}$

The bonding in $Se_6I_2^{2+}$ was examined by NBO and AIM analyses in the original paper **IV**. The AIM critical points found between iodine and dicoordinate selenium atoms (see Figure 12) indicated that the I···Se(dicoordinate) long contacts do have small bonding interactions, as suggested in previous studies. The calculated AIM bond orders and natural charges confirmed that the bond alternation observed in the $(Se_6I_2)[AsF_6]_2{\cdot}2SO_2$ crystal structure is intrinsic to the $Se_6I_2^{2+}$ cation and most likely due to the delocalization of the positive charge over the Se_6 ring.

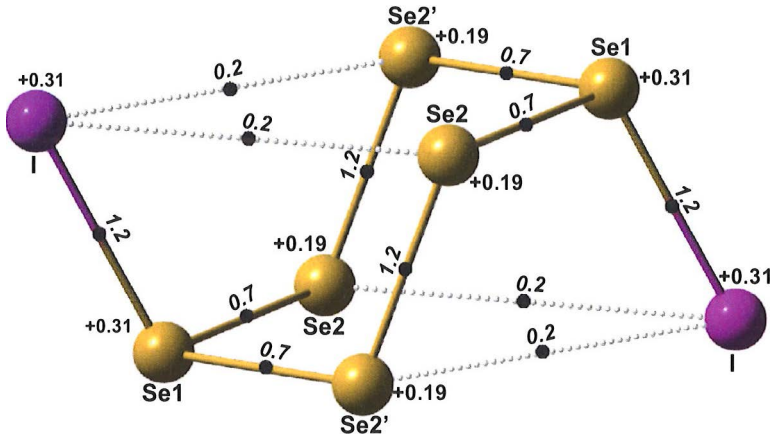

Figure 12. The bond critical points (black dots), relative AIM bond orders (bold), and natural atomic charges (bold italic) of the PBE0/(SDB)-cc-pVTZ optimized structure of $Se_6I_2^{2+}$.

The NBO description of the bonding of $Se_6I_2^{2+}$ illustrated in Figure 13 is in good agreement with the valence bond description presented previously in Figure 5. The NBO analysis effectively describes charge delocalization from the tricoordinate selenium atoms by p^2[Se(2)]→σ*[Se(1)-Se(2)] and p^2(I)→ σ*[Se(1)-Se(2)] types of electron transfers. The electron transfers decrease the strengths of the Se(1)-Se(2) bonds and increase the strengths of the Se(1)-I and the Se(2)-Se(2′) bonds, leading to the observed and calculated bond alternation.

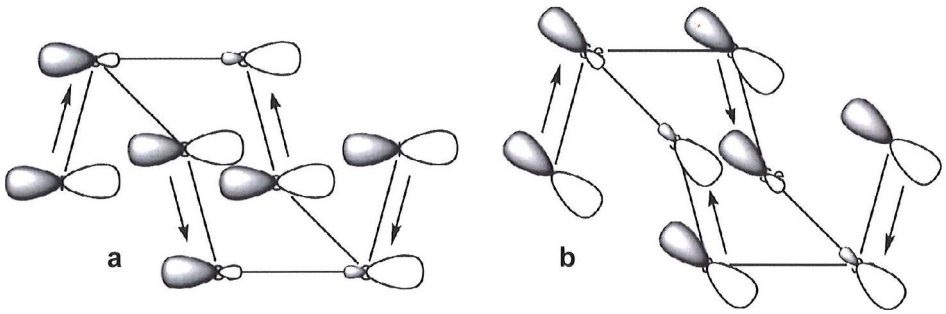

Figure 13. NBO description of the $p^2 \rightarrow \sigma^*$ type of electron transfer in $Se_6I_2^{2+}$. **a)** between p_x orbitals. **b)** between p_y orbitals.

2.4.6 The predicted structure of 1,1,4,4-$Se_4I_4^{2+}$

$Se_4I_4^{2+}$ has been characterized only in solution.[82] The characterization was based on a ^{77}Se NMR spectrum, which was consistent with an $I_2Se^+SeSeSe^+I_2$ chain structure. All attempts to grow crystals of $(Se_4I_4)[AsF_6]_2$ have been reported to have led to isolation of either $(SeI_3)[AsF_6]$ or $(Se_6I_2)[AsF_6]_2{\cdot}2SO_2$

crystals.[58,82] Since its experimental structure is still unknown, a theoretical structure of 1,1,4,4-$Se_4I_4^{2+}$ was calculated in the original paper **IV**. All attempts to optimize different conformations to 1,1,4,4-$Se_4I_4^{2+}$ resulted in the structure presented in Figure 14. The optimized structure of $Se_4I_4^{2+}$ is a chain that minimizes steric repulsion. The chain does not exhibit Se(1)···I long contacts that could be expected on the grounds of the structure of $Se_6I_2^{2+}$ (see Figure 12). However, bond alternation and charge delocalization are both present in the $Se_4I_4^{2+}$ chain as shown by calculated AIM bond orders and natural charges.

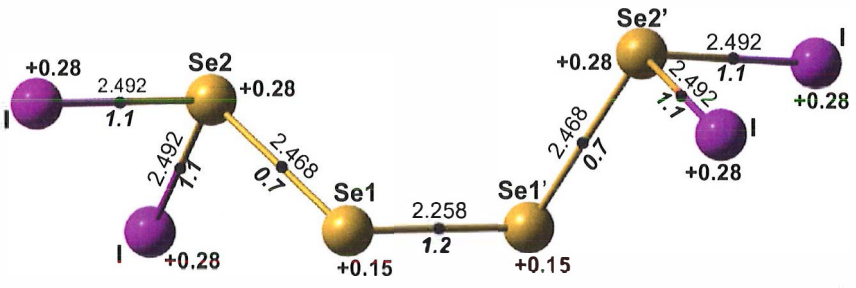

Figure 14. The PBE0/(SDB)-cc-pVTZ optimized structure of 1,1,4,4-$Se_4I_4^{2+}$.[IV] Bond lengths are given in Ångströms. Calculated natural charges (bold) and relative AIM bond orders (bold italic) are also shown.

2.4.7 Bonding in other calculated selenium iodine cations

In the second half of this thesis, theoretical ^{77}Se NMR calculations are used to aid the identification of previously unknown species observed in the reversible dissociation equilibrium of $(Se_6I_2)[AsF_6]_2$ in SO_2. Several selenium iodine structures were calculated in paper **IV** to account for the unknown species. The bonding in the optimized structures was studied with NBO and AIM analyses.

A general note from the bonding analyses was that all of the optimized structures exhibited similar structural features that were already found in previously characterized selenium and sulfur iodine cations. Selenium iodine bonds from formally positively charged selenium atoms were shorter than those expected for normal single bonds indicating partial π bonding and charge delocalization to iodine. Bond alternation that inferred charge delocalization via $p^2 \rightarrow \sigma^*$ type of electron transfers and presence of partial π bonds was apparent in all structures where there were chains of selenium atoms. From these observations it can be deduced that bond alternation, charge delocalization and preference for π bonds are not limited to the few structures so far characterized but are more likely common features of sulfur and selenium iodine cations.

3 THEORETICAL PREDICTION OF NMR PARAMETERS

The characterization of new species is currently routinely done using single crystal X-ray crystallography, provided that good quality crystals of the material are available. However, not all materials are crystalline. The synthesized products can be for example liquid or amorphous. In cases where X-ray crystallography cannot be used for characterization, spectroscopic methods come into play. NMR spectroscopy is a particularly powerful method for studying species in solutions. The parameters obtained from measured NMR spectra often contain enough information about the structure and the bonding in the species that they can be unequivocally characterized. This is true especially when there is a limited number of NMR active species present in the solution.

On the other hand there are many examples of species that take part in complex equilibrium mixtures in liquid phase (e.g. the sulfur-selenium binary system Se_nS_{8-n}).[83] The unambiguous identification of the components in these mixtures cannot rely solely on the experimental spectroscopic information. The interpretation of the spectroscopic information, however, can be greatly facilitated by a theoretical calculation of structures and a prediction of NMR parameters.

In the following sections, a short introduction to the methods and issues that are involved in the theoretical prediction of NMR parameters is presented.[84]

3.1 Theoretical background for NMR calculations

In atoms and molecules, the surrounding electrons modify the interactions that magnetic moments $\mathbf{M}_C$ of NMR active nuclei have with an external magnetic field $\mathbf{B}$. These modified interactions give rise to the observed NMR spectra that are used to identify different chemical species. Although the interactions themselves are rather complicated, the main features of the NMR

spectra can be accounted for by solving the energy equation for a simple effective spin-Hamiltonian:

$$H = -\sum_C \mathbf{B}^T (1 - \boldsymbol{\sigma}_C)\mathbf{M}_C + \tfrac{1}{2}\sum_{C \neq D} \mathbf{M}_C^T (\mathbf{D}_{CD} + \mathbf{K}_{CD})\mathbf{M}_D , \qquad (18)$$

where $\boldsymbol{\sigma}_C$ is the nuclear shielding tensor and $\mathbf{D}_{CD}$ and $\mathbf{K}_{CD}$ are the classical direct and the reduced indirect spin-spin coupling tensors, respectively. The nuclear shielding tensor $\boldsymbol{\sigma}_C$ describes how the surrounding electrons change the magnetic field felt by the nucleus C. The direct dipolar coupling tensor $\mathbf{D}_{CD}$ represents the direct coupling of the magnetic dipole moments of nuclei C and D and the reduced indirect spin-spin coupling tensor $\mathbf{K}_{CD}$ the indirect interaction of the nuclear magnetic dipole moments mediated by the surrounding electrons.

Molecules rotate freely in liquid and gas phases. The rotation of the molecules leads to a rotational averaging of the effective spin-Hamiltonian. Upon rotational averaging the direct couplings of the magnetic moments $\mathbf{D}_{CD}$ vanish but the indirect couplings $\mathbf{K}_{CD}$ do not. In a liquid phase the isotropic spin-Hamiltonian can be written as

$$H_{iso} = -\sum_C (1 - \sigma_C) B M_{C_z} + \tfrac{1}{2}\sum_{C \neq D} K_{CD} \mathbf{M}_C \cdot \mathbf{M}_D , \qquad (19)$$

where the nuclear shielding constants σ_C and the reduced indirect spin-spin coupling constants K_{CD} are defined as one third of the trace of the corresponding tensor.

The observed shieldings of nuclei are generally expressed in terms of the chemical shifts δ_C rather than the absolute shielding constants σ_C. The experimental chemical shifts are reported with respect to the chemical shift and the isotropic shielding constant of a suitable reference system:

$$\delta_C = \delta_{ref} + \sigma_{ref} - \sigma_C . \qquad (20)$$

The couplings between nuclei are given by the indirect spin-spin coupling constants J_{CD}, which are related to the reduced indirect spin-spin coupling constants via nuclear magnetogyric ratios γ_C:

$$J_{CD} = h \frac{\gamma_C}{2\pi} \frac{\gamma_D}{2\pi} K_{CD} . \qquad (21)$$

The numerical values of the empirical chemical shifts δ_C and the indirect spin-spin coupling constants J_{CD} are obtained from the measured spectra by fitting. Information of the structure and bonding in the molecular species can be derived from the fitted NMR parameters either directly or by comparison with the trends observed in the NMR spectra of previously characterized species.

Furthermore, if the structure of a molecular system is known and its electronic wavefunction can be determined, the chemical shifts and spin-spin coupling constants can be predicted theoretically and compared to the values extracted from experimental spectra.

3.1.1 NMR parameters as derivatives of energy

The energies associated with NMR transitions are exceedingly small compared to the total energies of electronic systems. This allows the calculation of NMR parameters as perturbations to the electronic wavefunction.

The total electronic energy of a molecular system changes in the presence of a perturbation. The changes in the total energy can be expressed in terms of a power series that is written with respect to the perturbation.[iv] In the presence of an external magnetic field and nuclear magnetic moments the energy of a closed shell system can be expanded around zero field and zero magnetic moments:

$$E(\mathbf{B},\mathbf{M}) = E_0 + \tfrac{1}{2}\mathbf{B}^T\mathbf{E}^{(20)}\mathbf{B} + \sum_C \mathbf{B}^T\mathbf{E}_C^{(11)}\mathbf{M}_K + \tfrac{1}{2}\sum_{C\neq D}\mathbf{M}_C^T\mathbf{E}_{CD}^{(02)}\mathbf{M}_D\,, \qquad (22)$$

where the energy derivatives are

$$\mathbf{E}^{(20)} = \left.\frac{d^2E(\mathbf{B},\mathbf{M})}{d\mathbf{B}^2}\right|_{\mathbf{B}=\mathbf{M}=0} \qquad (23)$$

$$\mathbf{E}_C^{(11)} = \left.\frac{d^2E(\mathbf{B},\mathbf{M})}{d\mathbf{B}d\mathbf{M}_C}\right|_{\mathbf{B}=\mathbf{M}=0} \qquad (24)$$

$$\mathbf{E}_{CD}^{(02)} = \left.\frac{d^2E(\mathbf{B},\mathbf{M})}{d\mathbf{M}_C d\mathbf{M}_D}\right|_{\mathbf{B}=\mathbf{M}=0} \qquad (25)$$

The first order terms vanish for a closed shell system and have not been included in the expression (22). The higher than second order terms are also neglected on account of their small sizes. The $\mathbf{E}^{(20)}$ tensor is the magnetizability of the molecule, which represents the direct interaction of the molecular system with the magnetic field. It does not enter the effective spin-Hamiltonian in equation (18). By combining the other two tensors $\mathbf{E}^{(11)}$ and $\mathbf{E}^{(02)}$ with the effective spin-Hamiltonian in equation (18) the following expressions are obtained for the magnetic shielding tensor and the indirect spin-spin coupling tensor, respectively:

[iv] The power series of energy E with respect to a perturbation $\mathbf{x}$ is: $E(\mathbf{x}) = E^{(0)} + \mathbf{E}^{(1)}\mathbf{x} + \tfrac{1}{2}\mathbf{x}^T\mathbf{E}^{(2)} + \cdots$, where $\mathbf{E}$ represents the response of the system to the perturbation. For a static perturbation, $\mathbf{E}$'s are obtained by differentiation at $\mathbf{x} = 0$, $\mathbf{E}^{(1)} = \left.\frac{dE}{d\mathbf{x}}\right|_{\mathbf{x}=0}$ and $\mathbf{E}^{(2)} = \left.\frac{d^2E}{d\mathbf{x}^2}\right|_{\mathbf{x}=0}$

$$\boldsymbol{\sigma}_C = \mathbf{E}_C^{(11)} + \mathbf{1} \tag{26}$$

$$\mathbf{K}_{CD} = \mathbf{E}_{CD}^{(02)} - \mathbf{D}_{CD} . \tag{27}$$

Theoretical magnetic shielding tensors and indirect spin-spin coupling tensors can thus be derived as derivatives of the total energy of the molecular system. The explicit expressions of these tensors as derivatives of energy will not be discussed here because the actual implementation of the NMR calculation methods is beyond the scope of this thesis. However, for an interested reader a good presentation of the equations required for a calculation of NMR parameters with a variety of different quantum chemical methods is given in a review by Helgaker et al.[85]

The following discussion concentrates on some of the practical aspects that should be considered in the calculations of isotropic magnetic shielding constants. The calculation of indirect spin-spin coupling constants is not covered here any further because they have not been calculated in the original research papers and the practical requirements for spin-spin coupling constant calculations are different from magnetic shielding calculations.

3.1.2 Gauge origin problem

One of the problems faced in the calculation of magnetic properties arises from the dependency that some of the operators have on the origin of the coordinate system.[22] The origin of the coordinate system is called gauge origin. In contrast to the operators, the calculated physical observables should be independent of the gauge origin and steps have to be taken to ensure this independency.

In particular, the kinetic energy operator **T** of a system,[v] which describes the movement of the electrons in the system, becomes dependent of the gauge origin in the presence of an external magnetic field. The external magnetic field interacts with the magnetic moments generated by the movement of the electrons and causes a perturbation to the kinetic energy. In the presence of this perturbation the kinetic energy operator **T** has the form

$$\mathbf{T} = \tfrac{1}{2}\left(-i\nabla - q\mathbf{A}\right)^2 = \tfrac{1}{2}\left(\mathbf{p} + \mathbf{A}\right)^2 , \tag{28}$$

where q is the charge of an electron (−1 in atomic units) and **A** is a vector potential associated with the magnetic field **B**. The magnetic field **B** is uniquely defined by the curl of the vector potential:[22,86]

$$\mathbf{B} = \nabla \times \mathbf{A} . \tag{29}$$

[v] The Hamiltonian operator can be written as the sum of the kinetic and the potential energies of a system: $\mathbf{H} = \mathbf{T} + \mathbf{V} = \frac{1}{2}(-i\nabla)^2 + \mathbf{V}$.

However, the vector potential **A** is not uniquely defined by the **B** because the gradient of an arbitrary scalar function can be added to **A** without changing the validity of the equation (29).[vi,86] One of the common ways to define **A** is

$$\mathbf{A} = \frac{1}{2}\mathbf{B} \times (\mathbf{r} - \mathbf{R}), \tag{30}$$

where **R** is the gauge origin. The gauge origin can be chosen arbitrarily. The choice of the gauge origin changes the Hamiltonian of the system and the eigenfunctions of the Hamiltonian (orbitals), but it should not affect the total wavefunction or the eigenvalues of the wavefunction since it does not change the magnetic field. In other words, the energy of the system and the derivatives of the energy (e.g. the nuclear magnetic shieldings) should be gauge origin independent. For exact wavefunctions the nuclear magnetic shieldings are indeed gauge origin independent because changing the gauge origin transforms the exact wavefunction as a proper unitary transformation. For example, a change of the gauge origin from **R** to **R′** transforms the wavefunction according to

$$\mathbf{A}_{\mathbf{R}'}(\mathbf{r}) = \mathbf{A}_{\mathbf{R}}(\mathbf{r}) + \frac{1}{2}\mathbf{B} \times (\mathbf{R} - \mathbf{R}') \cdot \mathbf{r} \tag{31}$$

$$\psi_{\mathbf{R}'}(\mathbf{r}) = \exp\left[-i\frac{1}{2}\mathbf{B} \times (\mathbf{R} - \mathbf{R}') \cdot \mathbf{r} \right] \psi_{\mathbf{R}}(\mathbf{r}) \ . \tag{32}$$

In contrast to exact wavefunctions, there is no guarantee for approximate wavefunctions expressed using finite basis sets that the wavefunctions are flexible enough to reproduce the transformation given in equation (32) exactly. The nuclear magnetic shieldings calculated with approximate wavefunctions can sometimes exhibit a very strong dependence on the choice of the gauge origin. Therefore the position of the gauge origin must always be reported for single gauge origin calculations.

For atomic calculations the nucleus provides a *natural* choice of the gauge origin.[86] On the other hand, there is no *natural* choice of the gauge origin for molecules and choosing a single gauge origin for molecular calculations is not recommended. Instead, for molecular systems all practical calculations use methods with distributed gauge origins that spread over the molecule. The distributed gauge origin methods ensure the proper transformation of the wavefunction upon a change of the gauge origin, for example, by including the complex phase factor in equation (32) either directly into atomic basis functions or into localized molecular orbitals. The gauge-including atomic orbital (GIAO) method is a popular distributed gauge origin method that incorporates the

[vi] The justification is that the curl of a derivative is always zero: $\nabla \times (\nabla \lambda) \equiv 0$, when λ is a scalar function.

complex phase factor into atomic basis functions.[vii,87] The individual gauge for localized orbitals (IGLO) method is an example of a distributed gauge method that is based on localized orbitals.[88] Other distributed gauge methods that have been developed to deal with the gauge origin problem include localized orbitals/localized origins (LORG),[89] individual gauges for atoms in molecules (IGAIM),[90] and continuous set of gauge transformation (CSGT)[91] methods, but these are used more seldom than the first two methods mentioned.

3.1.3 Basis sets for NMR parameter calculations

The choice of a basis set for practical calculations is always a tradeoff between accuracy and computational cost. This is even truer for heavier elements as the number of basis functions is apt to grow very fast as the quality of the basis set is improved. One of the common ways to restrict the rapid growth is to use effective core potential (ECP) basis sets.[24] In ECP basis sets the basis functions corresponding to the electrons that are closest to the nucleus are replaced by a core potential. Unfortunately, for NMR calculations, the ECP basis sets cannot be used on the atoms for which chemical shifts are calculated. NMR calculations probe the properties of wavefunctions in the core regions of atoms and ECPs are not good descriptions of the real behavior of wavefunctions near nuclei.[92] This makes it necessary to use all-electron basis sets at least on the atoms for which NMR properties are calculated.

The method used for solving the gauge origin problem dictates to a large extent the quality of the basis set required for shielding constant calculations. Even though all distributed gauge-origin methods (GIAO, IGLO, LORG, and CSGT) converge to the same isotropic shielding constant values, the basis set convergence of the GIAO results has been shown to be faster and smoother than that of any of the other methods.[87a,93] Consequently, the GIAO method was chosen in the original research papers **III** and **IV** for isotropic shielding constant calculations and the basis set requirements given here refer to GIAO calculations.

So far no systematic studies that compare the basis set convergence of shielding constant calculations between different basis set families have been reported in the literature.[85] Despite this, some general trends have been observed in the investigations that concentrated on different basis set families:[87a,94] 1) The accurate calculation of chemical shifts at the levels of theory that include electron correlation requires basis sets that are at least of triple zeta quality and 2) At least one set of polarization functions is needed in the calculation of chemical shieldings, 3) Diffuse functions have been shown to be important for chemical shielding calculations only if atoms have (partial) negative charges on them. Helgager et al.[85] have also pointed out that a basis set has to be flexible in the outer core region to produce reliable results for shielding constants. Therefore, basis sets with tightly contracted core functions, for example small correlation-consistent (e.g. cc-pVDZ) [95] and small ANO basis

[vii] The original name for GIAOs was London orbitals after the scientist who introduced them in 1937.[87c]

sets,[96] are poor choices for shielding constant calculations. Helgager et al. have considered the IGLO basis sets [88] and the larger ANO basis sets [96] to be good but computationally heavy choices for shielding calculations, and the Aldrichs TZP and QZP basis sets [97] to be good compromises for larger molecules.

In relativistic calculations the options for basis sets that can be chosen are somewhat reduced compared to non-relativistic calculations because relativistic methods generally require basis sets that have been optimized with the given relativistic approximation in mind.

3.1.4 Relativistic corrections in NMR calculations

The relativistic effects on the molecular properties of light elements like carbon or oxygen are usually negligible. In contrast, for species involving heavy elements beyond the fifth row of the periodic table, it is necessary to include relativistic corrections or use a relativistic theoretical framework in the calculation of molecular properties to produce results that are even qualitatively correct.[98] For some molecular properties such as shielding constants the relativistic treatment is required already at much smaller nuclear charges if results of high accuracy are desired.

Pyykkö et al.[99] have divided the relativistic effects that influence the calculated NMR shielding constants into two categories: The first category includes the effects that the presence of a heavy atom has on the nuclear shielding of a light neighbor atom (HALA effects). The second category consists of effects that describe how the relativity changes the nuclear shielding of the heavy atom (HAHA effects).

The use of relativistic ECP basis sets provides an efficient and easy way of implementing relativistic effects to most molecular calculations. The ECP basis sets can be readily used for treating the HALA effects on chemical shift calculations if information of the chemical shifts of the heavy atoms in the system is not required. There are several papers in the literature where chemical shifts for light elements (e.g. ^{1}H, ^{13}C, ^{17}O) in the presence of heavy elements have been successfully calculated by employing relativistic ECP basis sets on the heavy elements.[100] On the other hand, the ECP basis sets cannot be used to describe HAHA effects because the use of ECP basis sets prevents the calculation of meaningful NMR chemical shifts on the atoms for which they are used. To account for the relativistic effects in the chemical shifts of heavy atoms relativistic all electron methods have to be used.

One of the options for including relativistic effects in a shielding constant calculation is to treat the effects as another perturbation to the energy of a system and to write the relativistic corrections to the shielding constant in the form of a third order energy derivative:

$$\Delta\boldsymbol{\sigma}_C^{rel} = c^2 \left. \frac{d^3 E(\mathbf{B},\mathbf{M})}{d\mathbf{B} d\mathbf{M}_C dc^{-2}} \right|_{c\to\infty,\mathbf{B}=\mathbf{M}=0} \tag{33}$$

However, the usefulness of this approach is diminished by the fact that the relativistic effects on the shielding constants of the heaviest NMR nuclei can be huge and will not be fully covered by a perturbation that is linear in c^{-2}. A more practical way to calculate relativistic shielding constants is to use variational relativistic methods. Once a variational expression for the relativistic energy of a system is found, the shielding constants can be obtained as derivatives of the energy analogously to the non-relativistic case presented in section 3.1.1. The variational relativistic energy of an electron in an electromagnetic field is given by the Dirac operator **D**:[86]

$$\mathbf{D}\psi = \left(E + mc^2\right)\psi \tag{34}$$

$$\mathbf{D} = \boldsymbol{\beta}mc^2 + c\vec{\alpha}\cdot\left(\mathbf{p} + \mathbf{A}\right) + V\,, \tag{35}$$

where ψ is a four component relativistic wavefunction, $\boldsymbol{\beta}$ is a four by four Dirac matrix and $\vec{\alpha}$ is a vector of three Dirac matrices. The Dirac equation (34) can be written in a block form:

$$\left(\mathbf{D} - c^2\right)\psi = \begin{pmatrix} V & c\vec{\sigma}\cdot\left(\mathbf{p}+\mathbf{A}\right) \\ c\vec{\sigma}\cdot\left(\mathbf{p}+\mathbf{A}\right) & V - 2c^2 \end{pmatrix}\begin{pmatrix}\phi \\ \chi\end{pmatrix} = E\begin{pmatrix}\phi \\ \chi\end{pmatrix}, \tag{36}$$

where $\vec{\sigma}$ is a vector of three two by two Pauli matrices [viii] and ϕ and χ are called the large and the small component of the wavefunction, respectively. At the non-relativistic limit ($c \to \infty$) the large component ϕ of the electronic wavefunction reduces to the solutions of the corresponding non-relativistic equation (i.e. Schrödinger equation) and the small component χ vanishes.[22] The small component of the electronic wavefunction corresponds to a coupling with the positronic states (for which $E + mc^2 < 0$).

Solving the Dirac equation leads to fully relativistic four-component calculations. From a practical point of view these calculations are computationally very demanding. At the HF level, a four-component relativistic calculation is approximately a factor of a hundred more expensive than the corresponding non-relativistic calculation.[22] The four-component relativistic calculations of shielding constants have been restricted to atoms [101] and very small molecules (e.g. hydrogen halides).[102] The main application of the four-component results has been to use them as benchmark values for other more approximate relativistic calculations.[102]

In order to reduce the intrinsic computational requirements of the four-component calculations several approximate methods have been developed. Popular approximations have either treated the small component of the four-component wavefunction in an approximate way or formally eliminated it from the calculation, effectively reducing the components of the wavefunction into

---

[viii] The Dirac matrices and the Pauli matrices are related by $\boldsymbol{\alpha}_i = \begin{pmatrix} 0 & \boldsymbol{\sigma}_i \\ \boldsymbol{\sigma}_i & 0 \end{pmatrix}$.

two.[22] The oldest and probably the most well known two-component method is the Breit-Pauli method.[103] However, the Breit-Pauli calculations suffer from the highly singular behavior of the Breit-Pauli Hamiltonian near a nucleus and the resulting variational instability of the Hamiltonian.[104] Large frozen cores and basis sets that are very restricted in the core regions are required for heavy atoms to avoid the variational instability of the Breit-Pauli Hamiltonian.[98]

Variationally stable two-component methods are in general better choices for relativistic calculations than the Breit-Pauli method. There are currently two variationally stable methods that have been applied to nuclear shielding constants in molecules. The first one is the Hess's version of the second order Douglas-Kroll transformation (DKH2)[105] and the other one is the zeroth order regular approximation (ZORA).[106,107] In this thesis, the ZORA approximation is employed mainly because NMR calculations using density functional theory together with DKH2 method had not yet been implemented in any of the commercially available quantum chemistry packages at the time the computational work took place.

The two-component ZORA approximation can be derived from the four-component relativistic Dirac equation by writing the small component of the wavefunction given in equation (36) in terms of the large component $\chi = X\phi$.[106] This allows the formal elimination of the small component and gives the following eigenequation for the large component:

$$\left(V + c\vec{\sigma}\cdot(\mathbf{p}+\mathbf{A})X\right)\phi = E\phi \ , \tag{37}$$

where X can be written as

$$X = \left(\frac{c}{2c^2 - V}\right)\left(1 + \frac{E}{2c^2 - V}\right)^{-1} \vec{\sigma}\cdot(\mathbf{p}+\mathbf{A}). \tag{38}$$

By assuming that E << ($2c^2$−V), the large component eigenequation (37) can be expanded to zeroth order to give the ZORA Hamiltonian:

$$H^{ZORA} = \vec{\sigma}\cdot(\mathbf{p}+\mathbf{A})\frac{K}{2}\vec{\sigma}\cdot(\mathbf{p}+\mathbf{A}) + V \ , \tag{39}$$

where

$$K = \left[1 - V/2c^2\right]^{-1} \ .$$

The relativistic shielding tensor is obtained as a derivative of the ZORA energy. The explicit expressions for the energy derivatives are rather long and will not be given here but can be found in reference 107. Conceptually the relativistic shielding tensor can be divided into three parts:

$$\boldsymbol{\sigma}_C^{ZORA} = \boldsymbol{\sigma}_C^{d} + \boldsymbol{\sigma}_C^{p} + \boldsymbol{\sigma}_C^{SO} \tag{40}$$

The first two terms are the relativistic generalizations of the corresponding non-relativistic diamagnetic and paramagnetic shielding tensors, respectively.[107] They include the scalar relativistic (i.e. spin independent) corrections to the shielding tensor. The third term is spin dependent and gives a correction from the spin-orbit coupling to the shielding. The contribution from the spin-orbit correction to the shielding vanishes at the non-relativistic level for diamagnetic species.

Spin-orbit effects are agreed to be the main source for the observed HALA effects.[108] For example, the well-known normal halogen dependence of the chemical shifts is considered to be a result of the relativistic spin-orbit effects.[109] The normal halogen dependence refers to the increase in shielding of main group elements with increasing atomic number of halogen substituents and the increase in shielding with increasing number of halogen substituents. The strength of the normal halogen dependence has been attributed to the amount of s character in the bonds between the halogen substituents and the NMR active atoms.[110]

For shielding constant calculations of the heavy atoms themselves, both the scalar and the spin-orbit corrections have been shown to be of high importance.[98] In many cases, the trends that are obtained for heavy atom systems are dominated by the spin-orbit coupling, whereas scalar relativistic effects are of high importance in order to obtain the correct magnitudes of the heavy atom chemical shifts.

The ZORA and DKH2 methods have been shown to give similar results for a variety of molecular properties (e.g. binding energies, geometries, and vibrational frequencies) in the literature.[111] There is some evidence that the absolute shielding constants predicted with ZORA method tend to be smaller than the shielding constants predicted with DKH2 or four-component methods,[98,107,112] but this is not necessarily reflected as a better performance of the DKH2 method in predicting chemical shifts. In many cases the chemical shifts predicted with ZORA fit better with the experimental chemical shifts than the DKH2 chemical shifts (e.g. ^{119}Hg chemical shifts in $HgBr_2$, DFT ZORA 2684.4 ppm, HF DKH2 3462.1 ppm, Experimental 2213 ppm).[98] However, because there are also other effects that can have a strong influence on the accurate prediction of the chemical shifts of heavy atoms apart from the relativistic effects, it is not yet completely clear which method is the better choice for predicting chemical shifts.[98]

3.1.5 Solvent effects

The chemical shifts of apolar molecules in low-polarity solvents are reasonably well reproduced by *in vacuo* calculations.[113] However, in general the solvent effects on NMR spectra can be of considerable size. For example the ^{77}Se chemical shift of $SeCl_2$ can change from 1828 ppm in thf to 1748 ppm in CCl_4 and 1710 ppm in liquid mixture of $SeCl_2$, Se_2Cl_2 and $SeCl_4$, depending on the coordinating strength of the solvent.[III]

In recent years, a large number of methods have been proposed and employed for modeling the effects that solvents have on NMR chemical

shifts.[114] It is useful, from a theoretical point of view, to divide these methods into two categories: continuum solvation models, where the solvent is considered to be a macroscopic continuum dielectric characterized mainly by its dielectric constant, and discrete solvation models, where the microscopic structure of the solvent is retained and solvent molecules are explicitly included in the calculation.

Continuum solvation models partition a solution into two subunits: the solute molecule of interest and the surrounding solvent (see Figure 15).[115] The solute is described explicitly at a quantum mechanical level and is assumed to reside inside a cavity. The cavity is surrounded by a continuum medium which represents the solvent.[114] The solvent continuum is polarized by the presence of the solute molecule during a calculation. This polarization creates a reaction field, which in turn interacts with the electric field of the solute molecule and perturbs the molecular Hamiltonian of the solute. The main solute-solvent interaction is electrostatic, although some of the most recent continuum solvation models also include terms for non-electrostatic solute-solvent interactions.[115,116] The continuum solvation models are good for modeling the long-range electrostatic solvent effects and have been shown to improve the agreement of the calculated chemical shifts with the experimental chemical shifts for polar aprotic solvents.[113,117] On the other hand, for systems with explicit solute-solvent interactions such as hydrogen bonding the continuum solvent models are not equipped to reproduce correctly the effect of the solvent.[113-115]

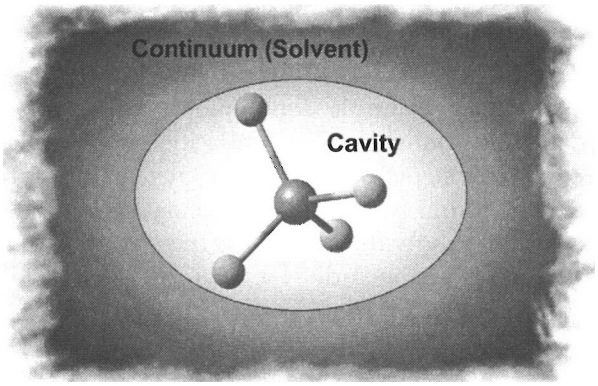

Figure 15. The continuum solvent methods place the solute molecule inside a cavity surrounded by a continuum representing the solvent. The cavity may be a sphere, an ellipsoid as shown in the figure, or a more complicated shape following the surface of the molecule.[114]

Discrete solvation methods are good for modeling the short-range explicit solute-solvent interactions.[113,114] In a discrete solvation calculation a solution is modeled by a molecular cluster where the solute molecule is surrounded by explicit solvent molecules. These clusters can be obtained either by a geometry

optimization or from a molecular dynamics simulation (using either classical potentials or *ab intio* Born-Oppenheimer or Car-Parrinello [118] type of simulations).[114] The sizes of the clusters that are derived from geometry optimizations are relatively limited compared to the clusters that can be produced by using molecular dynamics simulations. The optimized structures are good if a relatively few solvent molecules are strongly associated to the solute molecule of interest.[119] In these situations the surroundings of the solute molecule can be approximated by one rigid structure. On the other hand, if the interaction between the solute and the solvent is weaker, the situation in the solution is more dynamic and a variety of different representative structures can and do occur.[120] The dynamic conditions are better described by a set of structures obtained as snapshots of a molecular dynamics simulation taken at different time intervals. A shielding constant calculation is performed for each snapshot structure and the final shielding constants are calculated as statistical averages of the individual snapshots.

The discrete solvation calculations can in principle be used to model also the long-range solvent effects if enough solvent molecules are included in the cluster.[114] However, converged results with respect to the number of solvent molecules can require very large clusters.[121] The large cluster sizes impose restrictions on the methods that can be used to calculate the chemical shifts and thus limit the accuracy of the calculated chemical shifts.

The studies reported in the recent literature have mainly employed different combinations of the above continuum and discrete solvation methods.[113,119,122] These combination calculations have afforded the use of small clusters (only a few solvent molecules) to model the short-range solvation effects together with continuum solvation models to describe the long-range solvent effects leading to accurate chemical shift predictions with reasonable computational efforts. An example combination calculation can include as a first step a normal molecular dynamic simulation on a large cluster in order to derive the representative structures of the complete solute-solvent system.[120,121] In the second step, the actual chemical shift calculation, the bulk solvent effect is modeled by a continuum solvation method; the size of the molecular clusters can be drastically reduced to include just the solute molecule and a few of the closest solvent molecules. The requirement for only relatively small clusters also makes it possible to get good results using optimized cluster structures.[119,122]

Following the recent trend, a combination of small optimized solute-solvent clusters and COSMO continuum solvation model was used to describe the effect that the SO_2 solvent has on ^{77}Se chemical shifts of selenium iodine cations in paper **IV**.

3.2 Results and discussion

3.2.1 The experimental ^{77}Se NMR spectra of the reversible dissociation of $(Se_6I_2)[AsF_6]_2$ in liquid SO_2

The solvation of $(Se_6I_2)[AsF_6]_2$ to liquid SO_2 results in a complex equilibrium of cationic species. This equilibrium mixture was investigated in paper **IV** by ^{77}Se NMR spectroscopic measurements at −70 °C using both natural-abundance and ^{77}Se-enriched selenium. A ^{77}Se NMR spectrum of the equilibrium solution of the ^{77}Se-enriched sample is presented in Figure 16. The presence of 32 resonances in the NMR spectrum was established with the help of natural abundance spectra. A PS-DQF ^{77}Se-^{77}Se COSY spectrum shown in Figure 17 was used to demonstrate that the 32 resonances arise from 11 different cationic species. The observed spectra included resonances that had been assigned to Se_4^{2+}, Se_8^{2+}, Se_{10}^{2+}, SeI_3^+, 1,1,4,4-$Se_4I_4^{2+}$, and 1,4-$Se_6I_2^{2+}$ in previous studies. In addition, 22 other resonances belonging to five previously uncharacterized species **A-E** were found.

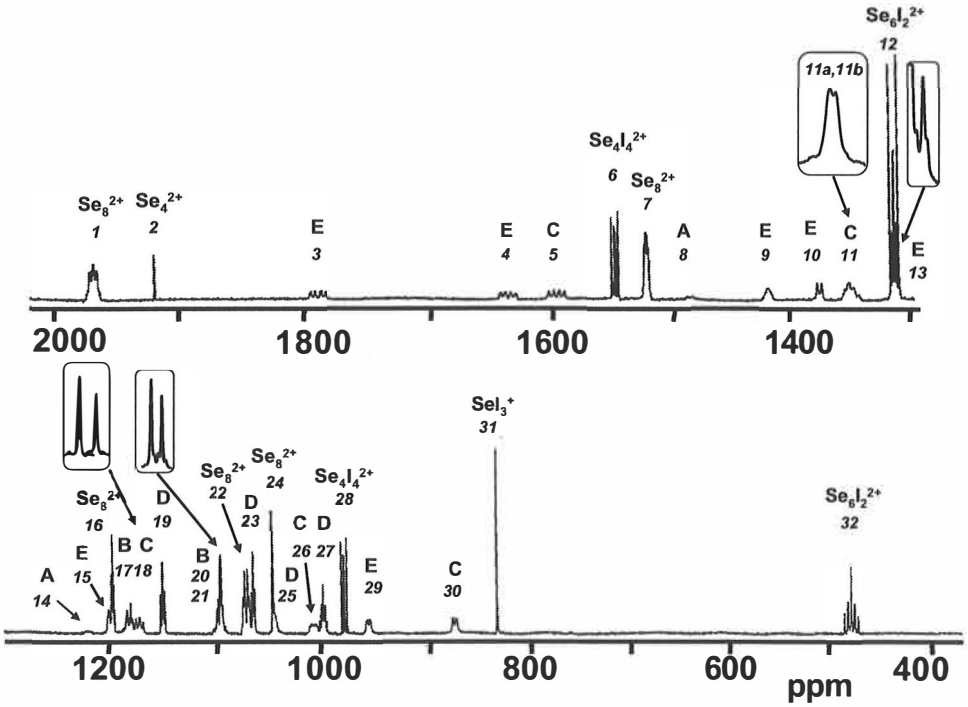

Figure 16. The ^{77}Se NMR spectrum of the equilibrium solution of ^{77}Se-enriched $Se_6I_2^{2+}$ in SO_2 (92 % enrichment level). Sections of natural abundance spectra are shown in inserts.

The simplest uncharacterized group of resonances **A** consists of two resonances 8 and 14. The resonances of group **A** have equal intensities and show coupling connectivity with each other but not with any other resonance.

The next group **B** arises from a six-spin system with three symmetry-related pairs of ^{77}Se nuclei giving resonances 17, 20, and 21 with equal intensities. There is a coupling correlation from resonance 17 to resonances 20 and 21 and between resonances 20 and 21. The six resonances of equal intensity (5, 11a, 11b, 18, 26, and 30) form the group **C**. Coupling correlation was observed between the resonances 5, 11a,b, and 26, as well as 11a,b, 18, and 30. Group **D** consists of four resonances 19, 23, 25, and 27 with relative intensities 2:2:1:2, respectively. There is coupling correlation from resonance 23, to resonances 25 and 27 and between resonances 19 and 27. The remaining seven resonances 3, 4, 9, 10, 13, 15, and 29 have equal intensities and constitute the last group **E.** The ^{77}Se-^{77}Se COSY spectrum shows coupling correlation from resonance 9 to resonances 13, 15, and 29, between resonances 4 and 10, and between resonances 3, 4, 9, and 13 confirming that they arise from the same species.

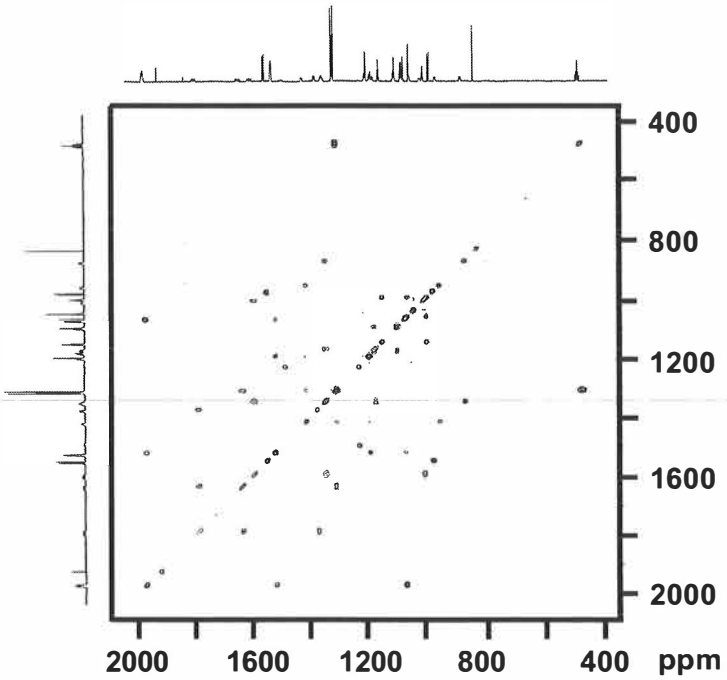

Figure 17. The PS-DQF ^{77}Se-^{77}Se COSY spectrum of the equilibrium solution of ^{77}Se-enriched $Se_6I_2^{2+}$ in SO_2.

3.2.2 Search for a reliable computational method for predicting ^{77}Se chemical shifts

Before ^{77}Se chemical shift calculations on the unknown **A-E** species were attempted, the reliability of the calculation methods was tested with a group of well-characterized selenium compounds in paper **III**. The set of reference species included SeX_2, SeX_3^+ (X = Cl, Br, I), SeR_2 (R = H, Me), Se_2X_2 (X = Cl, Br,

Me), Se_6, and Se_8. The isotropic shielding constant of the staggered-staggered conformation of $SeMe_2$ was adopted as the chemical shift reference point.

The performance of non-relativistic calculations was examined using MP2 calculations and DFT calculations with two different hybrid DFT functionals the B3PW91 and the PBE0. Two different basis sets were employed in the calculations: a Pople type 6-311G(d) basis set and a Dunning type cc-pVTZ basis set (SDB-cc-pVTZ for iodine). The influence of relativistic effects on the ^{77}Se chemical shifts was investigated with ZORA DFT calculations using the rPBE GGA functional and geometries optimized at a non-relativistic PBE0/cc-pVTZ level.

On the average, the non-relativistic methods produced the structures and the calculated vibrational frequencies of the reference species with good accuracy (for more details see paper **III**). The MP2 calculations seemed to be slightly more basis-set dependent than DFT calculations, but no significant differences were observed between the methods. On the other hand, the chemical shift calculations with MP2 method were feasible only for a few of the smallest species due to the high memory requirements of the calculations. The memory requirements hindered the usefulness of MP2 calculations for the purposes of the present study. The computed non-relativistic chemical shifts showed a good correlation with the experimental chemical shifts, aside from those calculated for selenium iodine species. For example, the computed chemical shift of SeI_3^+ was predicted to be 530 ppm too high by a PBE0/cc-pVTZ calculation.

The ZORA DFT calculations slightly improved the agreement between the computed and the experimental ^{77}Se chemical shifts for selenium iodine species compared to the non-relativistic calculations (e.g. the ^{77}Se chemical shift for SeI_3^+ was predicted to be 462 ppm too high by a ZORA calculation). However, the improvement came at the expense of a somewhat diminished overall accuracy of the calculated ^{77}Se chemical shifts. The diminished overall accuracy is in line with the general observation that the hybrid functionals reproduce chemical properties in a better agreement with experiment than the GGA functionals. The correlation of the chemical shifts calculated at the best non-relativistic level and at the relativistic level with the experimental chemical shifts is presented in Figure 18.

A further attempt to improve the calculated chemical shifts was made in paper **III** by adding the spin orbit part of the ZORA chemical shielding constant as a correction term [123] to non-relativistic PBE0/cc-pVTZ results. This combination method seemed to improve the correlation with experiment compared to ZORA results in the case of most references. However, the combination approach was disregarded in favor of the better-established ZORA calculations in paper **IV**.

Even with the inclusion of relativistic effects, the vacuum calculations did not seem to predict the ^{77}Se chemical shifts of selenium iodine species accurately enough to be useful in the identification of the unknown products of the reversible dissociation of $Se_6I_2^{2+}$. In a quest for more useful results the

influence of a solvent on the calculated chemical shifts of selenium iodine cations was investigated in paper **IV**. The effect of solvent was taken into account in calculations by using a combination of solvent models. The principal short-range solvent effects were treated by coordinating the iodine atoms of the cations with explicit solvent SO_2 molecules. As an example of the coordination, the coordination of SeI_3^+ by three SO_2 molecules is presented in Figure 19. In the case of the larger selenium-iodine cations and homoatomic selenium cations, additional SO_2 molecules were placed around the cations in an even manner. The structures of the clusters that resulted from the cations and the surrounding solvent molecules were fully optimized. Judging by how the SO_2 molecules arranged themselves around the cations during structure optimizations, the coordination of selenium atoms appears to be weaker than the coordination of iodine atoms. The long-range bulk solvent effects were incorporated using a COSMO continuum solvent model.

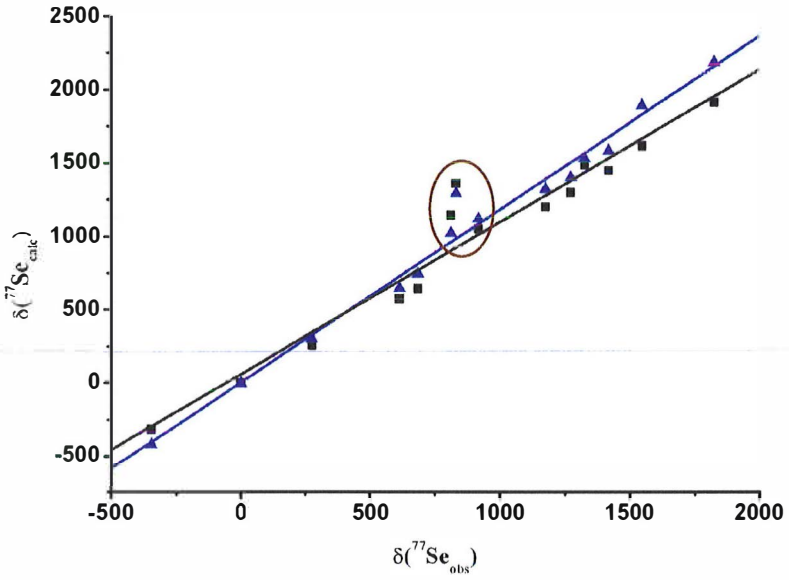

Figure 18. The correlation of chemical shifts calculated at a non-relativistic level (PBE0/cc-pVTZ; black squares) and a relativistic level (ZORA/rPBE/QZ4P; blue triangles) with the observed chemical shifts of small selenium compounds.[III] Data points that represent iodine containing species (Se_2I_2, SeI_2, and SeI_3^+) have been circled.

The inclusion of solvent effects significantly improved the agreement of computed chemical shifts with the experimental chemical shifts compared to vacuum calculations, and they helped us to suggest assignments for the unknown species more easily. For example, the computed ^{77}Se chemical shift of SeI_3^+ from a solvent ZORA calculation that used the cluster structure shown in Figure 19 is 1006 ppm, which is much closer to the experimental chemical shift

of 832 ppm than any of the values calculated *in vacuo*. Although the agreement is still not perfect, it is good enough to allow rudimentary comparisons between calculated structures to find out which species are most likely responsible for the observed chemical shifts.

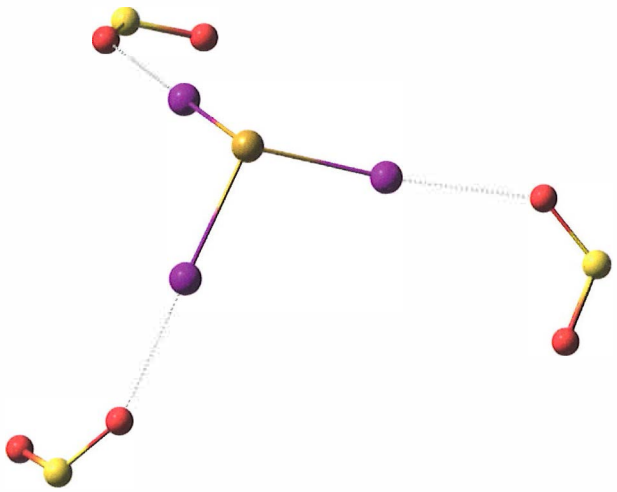

Figure 19. A cluster of SeI_3^+ and three SO_2 solvent molecules

The strong influence of solvent molecules on the calculated chemical shifts of selenium iodine cations raises the question whether adding counteranions to calculations would have a similar effect on the calculated chemical shifts. However, the counteranion in $(Se_6I_2)[AsF_6]_2$ is only weakly coordinating [II] and is most likely replaced by SO_2 molecules in solution. Therefore, AsF_6^- anions are expected to have only a minimal effect on the chemical shifts of selenium iodine cations and they have not been considered in the calculations.

3.2.3 Previously identified cations $Se_6I_2^{2+}$, $Se_4I_4^{2+}$, Se_4^{2+}, Se_8^{2+}, and Se_{10}^{2+}

The experimental information from ^{77}Se NMR spectra allows for two conformations of 1,4-$Se_6I_2^{2+}$ (*endo,endo* and *exo,exo*). The *endo,endo* conformation corresponds to the solid state structure presented in Figure 4 and the *exo,exo* conformation to a structure where the exocyclic iodine atoms adopt less hindered positions pointing away from the selenium ring. Both the *endo,endo* and the *exo,exo* were considered in paper **IV**. The different conformations were found to be close in energy. The *exo,exo* conformation is slightly more stable in the gas phase (by −3.5 kJ/mol), while in an SO_2 solution the *endo,endo* conformation was estimated to be lower in energy (by −15.7 kJ/mol). The energies indicate that 1,4-$Se_6I_2^{2+}$ retains its solid-state structure also in an SO_2 solution. The calculated ^{77}Se chemical shifts confirm this conclusion since the chemical shifts of the *endo,endo* conformation are much closer to the observed chemical shifts than the chemical shifts of the *exo,exo* conformation (see Table 2).

The calculated chemical shifts of 1,1,4,4-$Se_4I_4^{2+}$ do not exhibit quite as good an agreement with the observed chemical shifts as those calculated for $Se_6I_2^{2+}$.

However, the agreement is still reasonable and good enough to confirm the assignment of resonances 6 and 28 to 1,1,4,4-$Se_4I_4^{2+}$.

The ^{77}Se chemical shift of Se_4^{2+} has been calculated by Tuononen et al.[124] prior to this study. They have shown it to be necessary to use multiconfiguration methods to account for the electron correlation in Se_4^{2+} and to accurately predict its spectroscopic properties with *ab initio* calculations. Pure DFT calculations were also shown to give good ^{77}Se NMR chemical shifts for Se_4^{2+} and related four-membered ring cations. The ^{77}Se chemical shift calculated with the rPBE functional, which is a pure DFT functional, agreed very well with the observed chemical shift of Se_4^{2+}, in line with the results of Tuononen et al.

Table 2. The experimental and calculated ^{77}Se chemical shifts of 1,4-$Se_6I_2^{2+}$, 1,1,4,4-$Se_4I_4^{2+}$, SeI_3^+, Se_4^{2+}, and Se_8^{2+}.

Species	Atom number	Vacuum δ	Number of SO_2	Explicit solvent δ	Experimental δ	Res. no
endo,endo-$Se_6I_2^{2+}$	1	416	2	498	476	32
	2	1407		1319	1313	12
exo,exo-$Se_6I_2^{2+}$	1	688	2	674	476	32
	2	1778		1584	1313	12
$Se_4I_4^{2+}$	1	1596	4	1451	1548	6
	2	1163		1008	978	28
SeI_3^+	1	1294	3	1006	830	31
Se_4^{2+}	1	1925	4	1955	1922	2
Se_8^{2+}	1	1408	3	1330	1196 [a]	16
	2	1688		1630	1521	7
	3	2165		2028	1970	1
	4	1156		1127	1071	22
	5	1193		1175	1046	24

[a] The order of the chemical shifts is reversed compared to the original assignment of Burns et al.[125]

The ring structure of Se_8^{2+} has an *exo,endo* conformation as shown in Figure 20. The calculated ^{77}Se chemical shifts infer that the selenium atoms at the *exo* end of the cation are more shielded than those at the *endo* end; the observed chemical shifts are assigned accordingly in Table 2. Burns et al.,[125] who reported the measured ^{77}Se NMR spectra, suggested an opposite trend for the chemical shifts, where the selenium atoms at the *exo* end would be less shielded than the atoms at the *endo* end. The original assignment was based on one observed spin-spin coupling constant that agreed better with the original assignment than the assignment given here. However, changing the assignment of experimental chemical shifts from the one presented in Table 2 would make

the fit with the calculated chemical shifts drastically worse, which gives support for the assignment of Table 2 (see Paper **IV** for details).

Se_{10}^{2+} has been reported to exhibit only two NMR resonances, indicating that it is fluxional in solution.[125] The fluxionality prevents a simple comparison between the observed chemical shifts and those calculated for a fixed structure. A proper theoretical prediction of the chemical shifts of fluxional species requires the calculation of chemical shifts as statistical averages of several possible structures. Such a calculation was not attempted for Se_{10}^{2+}.

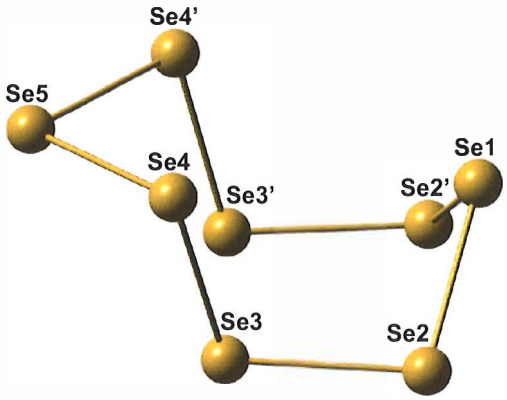

Figure 20. The optimized (PBE0/cc-pVTZ) structure of Se_8^{2+}.

3.2.4 Tentative identification of the spin-systems A-E

In order to assign the spin-systems **A-E**, the calculated chemical shifts, the balances of selenium, iodine, and charge in the course of the dissociation of $Se_6I_2^{2+}$, as well as the trends in the chemical shifts were considered in paper **IV**. A comparison of the experimental chemical shifts of spin systems **A-E** and the calculated chemical shifts of the cations proposed to account for the spin systems is presented in Table 3.

The two weak resonances of spin system **A** (see Figure 16) infer that they belong to a species, with at least two chemically inequivalent selenium atoms. 1,1,2-$Se_2I_3^+$(**1**) presented in Figure 21 is one of the simplest selenium iodine structures that can give the observed resonance pattern. The reasonable agreement between the calculated and experimental chemical shifts in Table 3 suggests that **1** is responsible for the resonances of spin system **A**.

The Se1 atom of 1,1,2-$Se_2I_3^+$ is a formally neutral selenium atom. By assigning the resonances of spin system **A** to **1**, it is acknowledged that despite the apparent instability of the bonds between neutral iodine and selenium atoms, binary species with such bonds can exist in a solution. Further justification for the existence of bonds between neutral iodine and selenium atoms is provided by the computational results given in paper **III**, which confirmed the experimental NMR results of Gopal and Milne [38] of finding SeI_2 and Se_2I_2 in CS_2.

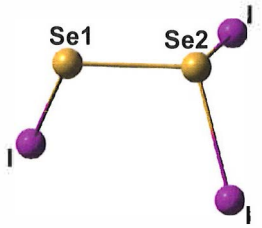

Figure 21. The optimized [PBE0/(SDB)-cc-pVTZ] structure of 1,1,2-$Se_2I_3^+$(**1**).

Table 3. The experimental ^{77}Se chemical shifts of the unknown spin-systems **A-E** and the calculated chemical shifts of the species suggested to account for the spin-systems.

Species	Atom no. [a]	Vacuum δ	No of SO_2	Explicit solvent δ	Experimental δ	I_{rel}	Reson. no. [b]
A	1	1456	3	1342	1486	32	8
($Se_2I_3^+$/**1**)	2	1005		973	1219	29	14
B	3,4	1660 [c]	6	1467 [c]	1181	104	17
($Se_6I_4^{2+}$/**2**)	5,6	1267 [c]		1054 [c]	1096	199	20
	1,2	1207 [c]		1101 [c]	1094		21
C	5	1637 [d]	3	1545 [d]	1597	46	5
($Se_6I_3^+$/**3**)	3	1174 [d]		1072 [d]	1351	47	11a
	4	1181 [d]		1089 [d]	1350	47	11b
	2	1298 [d]		1154 [d]	1170	43	18
	6	1127 [d]		1051 [d]	1007	48	26
	1	1024 [d]		883 [d]	873	42	30
D	4,5	1237 [e]	3	1142 [e]	1149	101	19
(Se_7I^+/**4**)	2,7	1299 [e]		1269 [e]	1064	100	23
	1	1289 [e]		1348 [e]	1044	obsc.	25
	3,6	1228 [e]		1207 [e]	998	98	27
E	2	1525	n.a.	n.a.	1791	44	3
[$(Se_7I)_2I^{3+}$/**5**]	3	1473		n.a.	1637	43	4
	5	1500		n.a.	1419	43	9
	4	1364		n.a.	1374	44	10
	1	1377		n.a.	1308	obsc.	13
	6	1013		n.a.	1200	43	15
	7	1005		n.a.	956	39	29

[a] For the numbering of atoms in the cations, see Figure 21 ($Se_2I_3^+$), Figure 22 ($Se_6I_4^{2+}$), Figure 23 ($Se_6I_3^+$), Figure 24 (Se_7I^+), and Figure 25 [$(Se_7I)_2I^+$]. [b] For the numbering of the resonances in the ^{77}Se NMR spectrum, see Figure 16. Calculated as averages of the chemical shifts of [c] three/ [d] two/ [e] four local minimum structures.

The resonance group **B** consists of three resonances with equal intensities. The resonance pattern suggests a species with six selenium atoms that form three magnetically equivalent pairs of selenium atoms. A 1,1,6,6-$Se_6I_4^{2+}$(**2**) chain was suggested in paper **IV** to account for the group **B**. The geometry optimization of 1,1,6,6-$Se_6I_4^{2+}$ yielded three low-energy local minima shown in Figure 22.

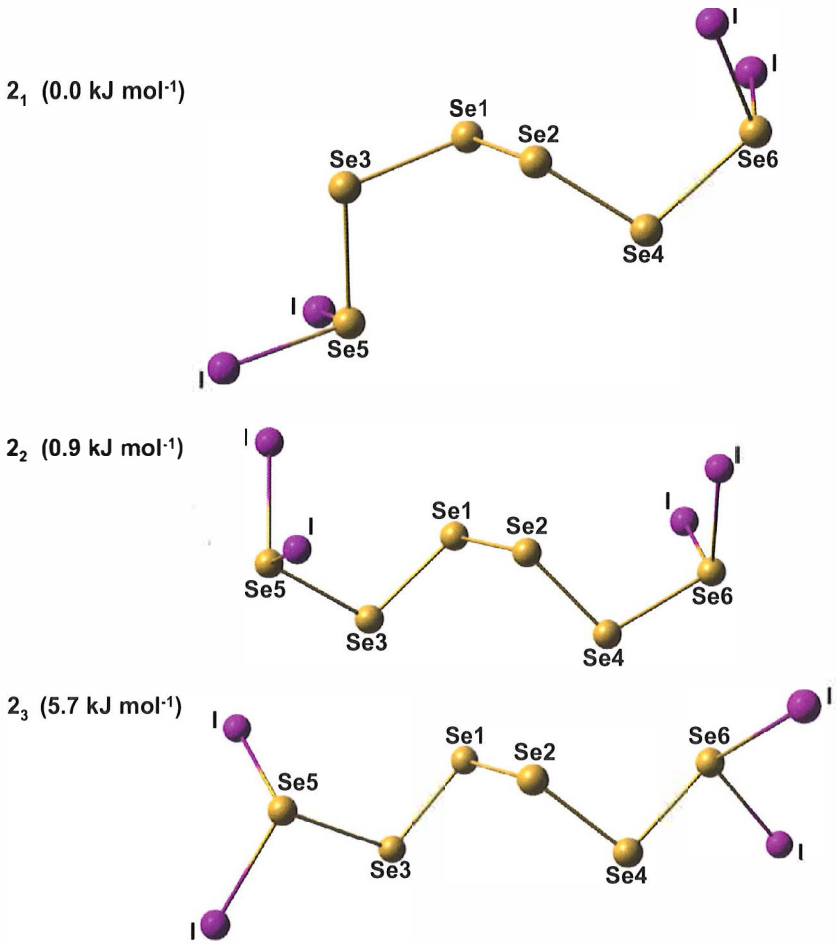

Figure 22. Three local minimum energy structures of 1,1,6,6-$Se_6I_4^{2+}$ (**2**) and their relative free energies in SO_2.

The three local minimum structures of **2** correspond to different orientations of the terminal SeI_2 units with respect to the chain of the four

central selenium atoms. The chain of the four central selenium atoms remains relatively unchanged from one structure to another. The asymmetric structure $\mathbf{2_1}$ has the lowest free energy in SO_2 solution; the other two conformations both with C_2 symmetry are slightly less stable.

Conforming to the optimized structure of $Se_4I_4^{2+}$, none of the structures of **2** show strong Se(dicoordinate)···I long contacts. The lack of Se(dicoordinate)···I long contacts is expected to facilitate the free rotation of the terminal SeI_2 in solution. The similarity of the relative energies of the three conformations makes it even more likely that the interconversion between the structures in solution is rapid. Rapid interconversion will render the structures indistinguishable within the time scale of NMR measurements. Therefore the experimental chemical shifts are compared in Table 3 with computed chemical shifts calculated as simple averages of the chemical shifts of the three conformations.

Apart from the chemical shifts calculated for the Se3 and Se4 atoms of **2**, the computed chemical shifts are in good agreement with the experimental ones. The explicit solvent calculations with six SO_2 molecules improve the agreement with the observed chemical shifts over vacuum results, but do not completely remove the discrepancy between the calculated and observed chemical shifts for atoms Se3 and Se4. However, given the simplicity of the theoretical model used for the treatment of the fluxionality of **2**, the calculated chemical shifts support the assignment of the group **B** resonances to 1,1,6,6-$Se_6I_4^{2+}$.

The simplest structure imaginable to account for the six resonances of group **C** that have equal intensities is an asymmetrical six-membered selenium chain. An asymmetrical 1,1,6,6-$Se_6I_4^{2+}$ structure corresponding to $\mathbf{2_1}$ was proposed in a preliminary experimental account [126] to give rise to the spin system **C**. However, in view of the computational results presented in paper **IV**, it seemed improbable that $\mathbf{2_1}$ would be responsible for **C**. An alternative six-selenium structure 1,1,6-$Se_6I_3^+$ (**3**) was suggested instead to account for the spin system.

The geometry optimization of **3** led to two local minimum structures that are presented in Figure 23. Conformation $\mathbf{3_2}$ lies 4.0 kJ mol^{-1} higher in energy than conformation $\mathbf{3_1}$. The energy difference is small enough to allow for both conformations to be in equilibrium in an SO_2 solution and to contribute to the observed chemical shifts. It is, therefore, more reasonable to use the averages of the chemical shifts of both conformations in comparisons with the observed chemical shifts. As shown in Table 3, the calculated average chemical shifts of **3** reproduce the correct trend for group **C** resonances. The coupling information reported in paper **IV** was also consistent with 1,1,6-$Se_6I_3^+$ and supported the assignment.

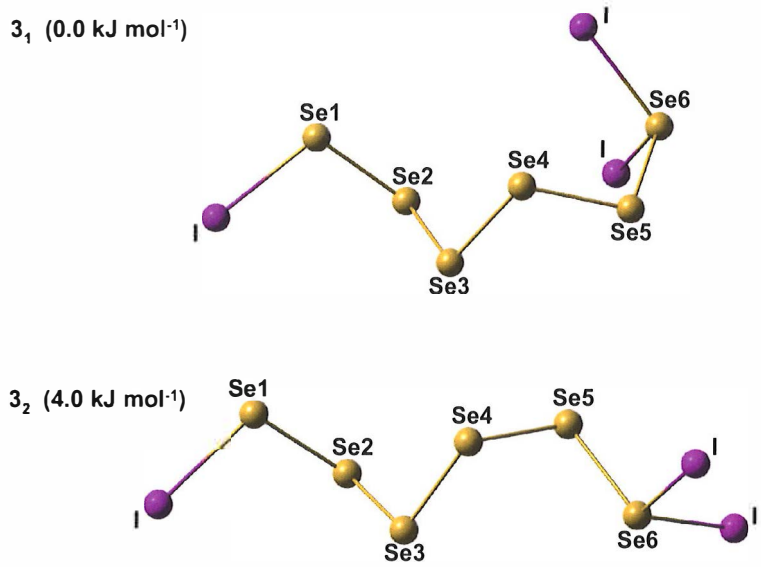

Figure 23. Two local minimum energy structures of 1,1,6-$Se_6I_3^+$ (**3**) and their relative free energies in SO_2.

The group **D** resonances cover a relatively small range and show a relative intensity pattern of 2:1:2:2, inferring a seven-spin ABB'CC'DD' system. The group **D** resonances were assigned to a cyclic Se_7I^+ (**4**), which was expected to be analogous to the S_7I^+ structure presented in Figure 6. The assignment of the otherwise C_1 -symmetric Se_7I^+ to four resonances can be rationalized by assuming that it goes through a pseudorotation in a similar manner to neutral seven-membered chalcogen ring molecules.[127] Four local minimum structures corresponding to different phases of the pseudorotation were found in the calculations; they are shown in Figure 24.

The pseudorotation of **4** is expected to be fast enough to equalize the chemical environments of the selenium atoms in a pairwise manner within the timescale of the NMR measurements. Consequently only four and not seven resonances are observed. In a similar manner to **2** and **3**, the averages of computed chemical shifts are compared with the experimental chemical shifts in Table 3. In contrast to **2** and **3**, the agreement between the observed and the calculated chemical shifts is only approximate for **4**. The worse agreement is attributed to the large changes that the pseudorotation inflicts on the chemical environments of the selenium atoms in **4**. Furthermore it is probable that there are other pseudorotation intermediates playing a significant role in the observed chemical shifts, explaining the differences between observed and calculated chemical shifts.

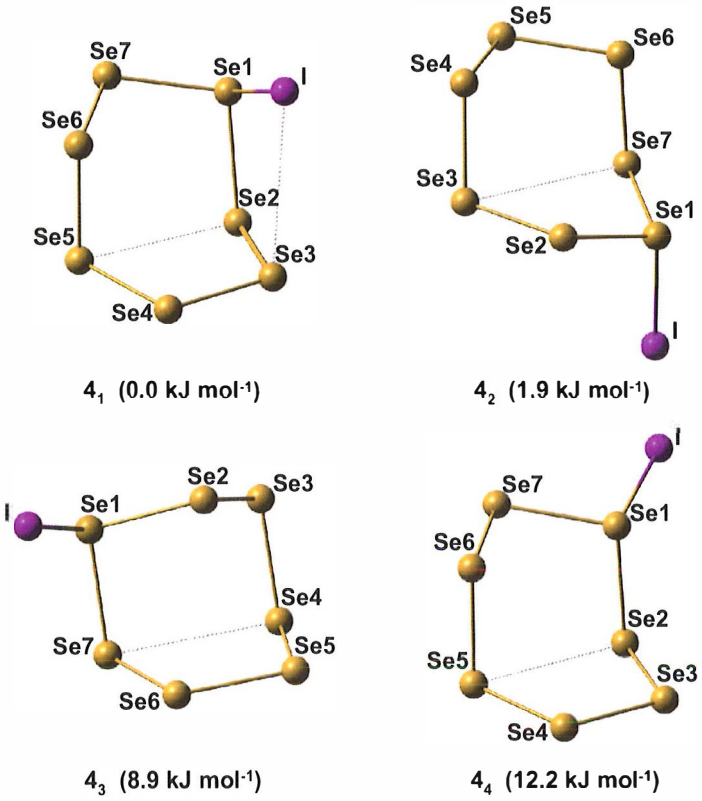

Figure 24. Four local minimum structures of Se_7I^+ (**4**) and their relative free energies in SO_2 solution.

The seven resonances of group **E** have equal intensities. This indicates that group **E** arises from a species that has seven magnetically inequivalent selenium atoms. Because the seven-membered selenium ring structures are expected to exhibit pseudorotation in an SO_2 solution, the selenium analog of $[(S_7I)_2I]^{3+}$ was considered as a candidate to account for the spin system **E**. The optimized geometry of $[(Se_7I)_2I]^{3+}$ (**5**) presented in Figure 25 differs somewhat from the experimental conformation of $[(S_7I)_2I]^{3+}$ given in Figure 7. The differences between the geometries of $[(Se_7I)_2I]^{3+}$ and $[(S_7I)_2I]^{3+}$ are attributed to crystal packing forces, which would favor the more compact conformation of $[(S_7I)_2I]^{3+}$ in the solid state.

The assignment of spin system **E** to **5** can be rationalized as follows. The bonding of the Se_7 rings to inequivalent iodine atoms in **5** ensures that the selenium atoms within the rings remain magnetically inequivalent despite the possible pseudorotation of the Se_7 rings. It is, furthermore, assumed that the two Se_7 rings of **5** are equivalent in an SO_2 solution and the quadrupolar iodine atom between the two Se_7 rings does not carry coupling information. Keeping the above assumptions in mind the calculated vacuum chemical shifts shown in Table 3 are in good agreement with the observed resonances.

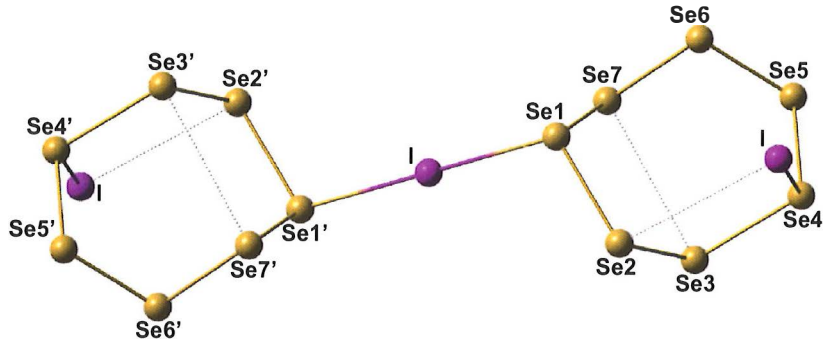

Figure 25. The optimized [PBE0/(SDB)-cc-pVTZ] structure of $[(Se_7I)_2I]^{3+}$ (**5**).

Explicit solvent results have not been presented for **5**. Due to the expected fluxionality and the large size of the cation, calculations with enough explicit solvent molecules to yield a balanced description of the solvent surroundings were not feasible with the computational resources available. The structural assignment was shown to yield reasonable coupling information for **5** in paper **IV**, giving confidence to the assignment.

The assignment of spin systems **A**-**E** presented here assumes that all of the selenium and iodine from $Se_6I_2^{2+}$ is present in the species observed in the ^{77}Se NMR spectra. Support for this assumption and the present assignment was given by a consideration of iodine, selenium and charge balances calculated from the relative integrated intensities of the measured ^{77}Se NMR chemical shifts (see paper **IV** for more information). The calculated balances indicated that within the accuracy of the experimental results, the suggested cations account for all of the initial selenium, iodine and positive charge. In conclusion the assignment presented here can be considered reasonable, even though the possibility that the spin systems **A**-**E** represent some other cations cannot be completely ruled out.

3.2.5 The quality of the calculated chemical shifts

At best, the calculated chemical shifts presented in Tables 2 and 3 are remarkably close to the observed chemical shifts. This is especially true for the chemical shifts calculated for $Se_6I_2^{2+}$. On the other hand, some of the calculated chemical shifts differ from the observed ones by several hundred ppm. Large differences are noted especially for species expected to be fluxional in a solution. The explicit solvent calculations appear to improve the general agreement between the observed resonances and the calculated chemical shifts, but some large discrepancies still remain.

The chemical shifts calculated for the previously characterized species agree somewhat better with the observed resonances than those calculated for the cations suggested to account for the spin systems **A**-**E**. Some of the

differences can be attributed to the expected fluxionality of the new cations and the inability of the calculation method to fully model the fluxionality and the solvent environment. Unfortunately the large differences also mean the possibility that the spin systems **A**-**E** represent other cations than the ones suggested here. Therefore the assignment of the new species remains tentative and more work is needed to confirm it.

Despite the shortcomings of the present calculations, the ongoing development of better calculation methods provides hope of finding a definite answer to the identity of spin systems **A**-**E** in the near future. The increase in computational resources allows for the calculation of larger clusters, thus improving the description of cations in solution. The development of new density functionals is anticipated to overcome the difficulties associated with the modeling of long range interactions.[26] This would remove the uncertainty in the modeling of the weak selenium iodine contacts that were expected, but are not found, in the majority of the cations studied in the present calculations. The statistically averaged results from Car-Parrinello type of molecular dynamics simulations could also provide an attractive alternative to the present geometry optimizations.

4 CONCLUSIONS

Conceptual bonding models are important tools in chemistry because they allow the fast rationalization of the properties and the chemical behavior of new structures. A good conceptual bonding model is simple to use; it explains the observed structures and their behavior, and it conforms to the results of more advanced theoretical models.

In this thesis the simple bonding concepts derived in the literature to explain the observed structures of sulfur and selenium iodine cations were tested against more rigorous theoretical models of bonding. For example, the concepts of delocalization of positive charge via bond alternation leading to stabilization of structures due to a diminished Coulomb repulsion, and the formation of π^*- π^* bonds were, confirmed to be at least qualitatively correct and able to explain the observed bond lengths and other structural features of the studied cations. The validation of these simple bonding concepts gives theoretical support for their use in explaining various kinds of bonding situations presented in recent literature.

The differences of the bonding in the simplest selenium and sulfur iodine cations were examined with theoretical calculations. The bonding in SeI_3^+ was compared to that in the non-existent SI_3^+ and the bonding in $Se_2I_4^{2+}$ to that in $S_2I_4^{2+}$. The differences between these structures were attributed mainly to the high strength of the sulfur-sulfur π bond relative to the other types of bonds available. The high strength of the sulfur-sulfur π bond not only leads to different structures for $Se_2I_4^{2+}$ and $S_2I_4^{2+}$, but also to the non-existence of SI_3^+. Due to the strength of the sulfur-sulfur π bond compared to the sulfur-iodine bond, SI_3^+ is not stable towards the formation of $S_2I_4^{2+}$ in the synthesis conditions, whereas SeI_3^+ is preferred over $Se_2I_4^{2+}$ in a solution if enough iodine is present. The results presented here for the small sulfur and selenium iodine cations provide a theoretical basis for the study of the differences in the larger cations and for finding general causes for the differences. Perhaps even some tools can be found leading to the first stabilization of a structural selenium analog of a sulfur iodine cation in the solid state or vice versa.

The results presented for the calculation of the ^{77}Se NMR chemical shifts of selenium iodine cations emphasize the importance of taking into account the relativistic effects and the effects due to the solution environment. The inclusion of relativistic contributions to ^{77}Se chemical shifts was shown to be particularly important in cases where selenium is bonded to a heavier element such as iodine. The efficient modeling of the influence of the surrounding solution medium on the chemical shifts was established to require both the inclusion of explicit solvent molecules and the use of continuum solvation models.

Theoretical ^{77}Se NMR chemical shift calculations have been used to aid the interpretation of the experimental data from the equilibrium solution of the reversible dissociation of $(Se_6I_2)[AsF_6]_2$ in SO_2. With the aid of theoretical chemical shift predictions, the existence of previously unknown 1,1,2-$Se_2I_3^+$, 1,1,6,6-$Se_6I_4^{2+}$, 1,1,6-$Se_6I_3^+$, Se_7I^+, and $(Se_7I)_2I^{3+}$ cations has been inferred in an SO_2 solution. The calculations were very helpful in determining the cations that most likely take part in the equilibrium solution of the reversible dissociation of $(Se_6I_2)[AsF_6]_2$. However, the results also showed how difficult it is to find an unambiguous assignment for a complex mixture of species using the limited information provided by a single NMR active nucleus. For compounds of heavier elements relativistic effects, solvent effects, and the interchange between several energetically similar conformations play important roles. For these compounds the calculation of chemical shifts still does not facilitate unambiguous spectral assignments based only on comparison of experimental and calculated chemical shifts. Therefore, more development work in computational methodology is still required.

REFERENCES

1 Dasent, W. E. *Non-Existent Compounds: Compounds of Low Stability*, Marcel Dekker: New York, 1965, p. 162.

2 Klapötke, T.; Passmore, J. *Acc. Chem. Res.* **1989**, *22*, 234.

3 Krebs, B.; Ahlers, F.-P. *Adv. Inorg. Chem.* **1990**, *35*, 235.

4 Reed, A. E.; Curtiss, L. A.; Weinhold, F. *Chem. Rev.* **1988**, *88*, 899.

5 Kaupp, M.; Bühl, M.; Malkin, V. G. (Eds.), *Calculation of NMR and EPR Parameters: Theory and Applications*, Wiley VCH, 2004.

6 Bader, R. W. F. *Atoms in molecules – A quantum theory*, Oxford University Press: Oxford, 1990.

7 (a) Silvi, B.; Savin,A. *Nature* **1994**, 371, 683. (b) Becke, A. D.; Edgecombe, K. E. *J. Chem. Phys.* **1990**, *92*, 5397.

8 (a) Reed, A. E.; Weinstock, R. B.; Weinhold, F. *J. Chem. Phys.* **1985**, *83*, 735. (b) Reed, A. E.; Weinhold, F. *J. Chem. Phys.* **1983**, *78*, 4066;

9 Macchi, P.; Sironi, A. *Coord. Chem. Rev.* **2003**, *238-239*, 383.

10 Bader, R. F. W.; Johnson, S.; Tang, T.-H.; Popelier, P. L. A. *J. Phys. Chem.* **1996**, *100*, 15398.

11 Gillespie, R. J.; Popelier, P. L. A. *Chemical Bonding and Molecular Geometry – From Lewis to Electron Densities*, Oxford University Press: New York, 2001.

12 (a) Cremer, D.; Kraka, E. *Angew. Chem.* **1984**, *96*, 612; *Angew. Chem., Int. Ed. Engl.* **1984**, *23*, 627. (b) Cremer, D.; Kraka, E. *Croat. Chem. Acta* **1985**, *57*, 1259.

13 Bader, R. W. F.; Stephens, M. E. *J. Am. Chem. Soc.* **1975**, *97*, 7391.

14 (a) Fradera, X.; Poater, J.; Simon, S.; Duran, M.; Solà, M. *Theor. Chem. Acc.* **2002**, *108*, 214. (b) Fradera, X.; Austen, M. A.; Bader, R. W. F. *J. Phys. Chem. A* **1999**, *103*, 304.

15 Bader, R. F. W.; Matta, C. F. *J. Phys. Chem. A* **2004**, *108*, 8385.

16 Power, P. P. *Chem. Rev.* **1999**, *99*, 3463.

17 (a) Bridgeman, A. J.; Ireland, L. R. *Polyhedron* **2001**, *20*, 2841. (b) Landis, C. R.; Weinhold, F. *J. Am. Chem. Soc.* **2006**, *128*, 7335.

18 Sekiguchi, A.; Kinjo,R.; Ichinohe,M. *Science* **2004**, *305*, 1755.

19 (a) Molina Molina, J.; Dobado, J. A.; Heard, G. L.; Bader, R. F. W.; Sundberg, M. R. *Theor. Chem. Acc.* **2001**, *105*, 365. (b) Malcolm, N. O. J.; Gillespie, R. J.; Popelier, P. L. A. *J. Chem. Soc., Dalton Trans.* **2002**, 3333. (c) Chesnut, D. B. *Heteroat. Chem.* **2003**, *14*, 175.

20 Koch, W.; Holthausen, M. C. *A Chemist's Guide to Density Functional Theory*, 2nd ed., John Wiley & Sons: Chichester, UK, 2001.

21 Hohenberg, P.; Kohn, W. *Phys. Rev.* **1964**, *136*, B864.

22 Jensen, F. *Introduction to Computational Chemistry*, John Wiley & Sons: Chichester, UK, 1999.

23 Kohn, W.; Sham, L. J. *Phys. Rev.* **1965**, *140*, A1133.

24 Young, D. C. *Computational Chemistry: A Practical Guide for Applying Techniques to Real-World Problems*, Wiley-Interscience: New York, 2001.

25 Slater, J. C. *Phys. Rev.* **1951**, *81*, 385.

26 Jurečka, P.; Černý, J.; Hobza, P.; Salahub, D. R. *J. Comput. Chem.* **2007**, *28*, 555.

27 Kurth, S.; Perdew, J. P.; Blaha, P. *Int. J. Quantum Chem.* **1999**, *75*, 889.

28 (a) Becke, A. D. *J. Chem. Phys.* **1996**, *104*, 1040. (b) Boese, A. D.; Martin, J. M. L. *J. Chem. Phys.* **2004**, *121*, 3405. (c) Zhao, Y.; Lynch, B. J.; Truhlar, D. G. *Phys. Chem. Chem. Phys.* **2005**, *7*, 43.

29 (a) Grimme, S. *J. Chem. Phys.* **2006**, *124*, 034108. (b) Neese, F.; Schwabe, T.; Grimme, S. *J. Chem. Phys.* **2007**, *126*, 124115.

30 (a) Schultz, N. E.; Zhao, Y.; Truhlar, D. G. *J. Phys. Chem. A* **2005**, *109*, 11127. (b) Riley, K. E.; Op't Holt, B. T.; Merz, K. M. *J. Chem. Theory Comput.* **2007**, *3*, 407.

31 Perdew, J. P.; Burke, K.; Ernzerhof, M. *Phys. Rev. Lett.* **1996**, *77*, 3865; **1997**, *78*, 1396 (E).

32 (a) Perdew, J. P.; Ernzerhof, M.; Burke, K. *J. Chem. Phys.* **1996**, *105*, 9982. (b) Adamo, C.; Barone, V. *J. Chem. Phys.* **1999**, *110*, 6158.

33 (a) Perdew, J. P.; Wang, Y. *Phys. Rev.* **1992**, *B45*, 13244. (b) Becke, A. D. *J. Chem. Phys.* **1993**, *98*, 5648.

34 (a) Adamo, C.; Barone, V. *Chem. Phys. Lett.* **1997**, *274*, 242. (b) Adamo, C.; Barone, V. *J. Chem. Phys.* **1998**, *108*, 664.

35 Hammer, B.; Hansen, L. B.; Nørskov, J. K. *Phys. Rev.* **1999**, *B59*, 7413.

36 Krummel, G.; Minkwitz, R. *Inorg. Nucl. Chem. Lett.* **1977**, *13*, 213.

37 Feuerhahn, M.; Vahl, G. *Inorg. Nucl. Chem. Lett.* **1980**, *16*, 5.

38 Gobal, M.; Milne, J. *Inorg. Chem.* **1992**, *31*, 5430.

39 Pauling, L. *The Nature of the Chemical Bond*, 3rd ed., Cornell University Press: New York, 1960.

40 Johnson, J. P.; Murchie, M.; Passmore, J.; Tajik, M.; White, P. S.; Wong, C.-M. *Can. J. Chem.* **1987**, *65*, 2744.

41 Goto, K.; Holler, M.; Okazaki, R. *Chem. Comm.* **1998**, 1915.

42 du Mont, W.-W.; Kubiniok,S.; Peters, K.; Von Schnering, H. G. *Angew. Chem.* **1987**, *99*, 820; *Angew. Chem., Int. Ed. Engl.* **1987**, *26*, 780.

43 (a) Greenwood, N. N.; Straughan, B. P. *J. Chem. Soc. A* **1966**, 962. (b) Hendra, P. J.; Jovic, Z. *J. Chem. Soc. A* **1968**, 600.

44 Passmore, J.; Taylor, P. *J. Chem. Soc., Dalton Trans.* **1976**, 804.

45 Johnson, J. P.; Murchie, M.; Passmore, J.; Tajik, M.; White, P. S.; Wong, C.-M. *Can. J. Chem.* **1987**, *65*, 2744

46 (a) Murchie, M. P.; Johnson, J. P.; Passmore, J.; Sutherland, G.; Tajik, M.; Whidden, T. K.; White, P. S.; Grein, F. *Inorg. Chem.* **1992**, *31*, 273. (b) Passmore, J.; Sutherland, G.; Whidden, T. K.; White, P. S. *Chem. Commun.* **1980**, 289.

47 (a) Zak, Z.; Cernik, M. *Acta Crystallogr.* **1996**, *C52*, 290. (b) Leung, Y. C.; Waser, J. *J. Phys. Chem.* **1956**, *60*, 539.

48 Skabara, P. J.; Berridge, R.; Bricklebank, N.; Lath, H.; Coles, S. J.; Horton, P. N. *Polyhedron* **2006**, *25*, 989.

49 Cristiani, F.; Devillanova, F. A.; Isaia, F.; Lippolis, V.; Verani, G.; Demartin, F. *Polyhedron* **1995**, *14*, 2937.

50 Nandana, W. A. S.; Passmore, J.; White, P. S.; Wong, C.-M. *Chem. Commun.* **1982**, *19*, 1098.

51 Nandana, W. A. S.; Passmore, J.; White, P. S.; Wong, C.-M. *Inorg. Chem.* **1990**, *29*, 3529.

52 Cherin, P.; Unger, P. *Acta Crystallogr.* **1972**, *28*, 313.

53 Faggiani, R.; Gillespie, R. J.; Kapoor, R.; Lock, C. J. L.; Vekris, J. E. *Inorg. Chem.* **1988**, *27*, 4350.

54 Passmore, J.; Taylor, P.; Whidden, T.; White, P. S. *Can. J. Chem.* **1979**, *57*, 968.

55 (a) Kiers, C. T.; Vos, A. Acta Crystallogr. **1978**, *B34*, 1499. (b) Dunitz, J. D. *Acta Crystallogr.* **1956**, 579.

56 Passmore, J.; White, P. S.; Wong, C.-M. *Chem. Commun.* **1985**, 1178.

57 Nandana, W. A. S.; Passmore, J.; White, P. S.; Wong, C.-M. *Inorg. Chem.* **1989**, *28*, 3320.

58 Passmore, J. Homopolyatomic Selenium Cations and Related Halo-Polyselenium Cations. In Steudel, R. (Ed.) *Studies in Inorganic Chemistry*, 14, Elsevier: New York, 1992.

59 Nandana, W. A. S.; Passmore, J.; White, P. S. *Chem. Commun.* **1983**, 526.

60 Maddox, H.; McCullough, J. D. *Inorg. Chem.* **1966**, *5*, 522.

61 Passmore, J.; Taylor, P.; Whidden, T. K.; White, P. *Chem. Commun.* **1976**, 689.

62 Passmore, J.; Sutherland, G.; Taylor, P.; Whidden, T. K.; White, P. S. *Inorg. Chem.* **1981**, *20*, 3839.

63 Passmore, J.; Sutherland, G.; White, P. S. J. Chem. Soc., *Chem. Commun.* **1980**, 330.

64 (a) Steudel, R.; Steidel, J.; Pickardt, J.; Schuster, F.; Reinhardt, R. Z. *Naturforsch.* **1980**, *35B*, 1378. (b) Steudel, R.; Reinhardt, R.; Schuster, F. Angew. Chem., Int. Ed. Engl. **1977**, *16*, 715; *Angew. Chem.* **1977**, *89*, 756.

65 Steudel, R.; Reinhardt, R.; Sandow, T. *Angew. Chem., Int. Ed. Engl.* **1977**, *16*, 716; *Angew. Chem.* **1977**, *89*, 757.

66 Minkwitz, R.; Preut,H.; Sawatzki,J. Z. *Naturforsch.* **1988**, *43B*, 399.

67 Passmore, J.; Sutherland, G.; White, P. S. *J. Chem. Soc., Chem. Commun.* **1979**, 901.

68 Lin, G. H. Y.; Hope, H. *Acta Crystallogr.* **1972**, *B28*, 643.

69 (a) Pignedoli, C. A.; Curioni, A.; Andreoni, W. *ChemPhysChem*, **2006**, *7*, 801. (b) Frenking, G.; Krapp, A.; Nagase, S.; Takagi, N.; Sekiguchi, A. *ChemPhysChem*, **2006**, *7*, 799. (c) Pignedoli, C. A.; Curioni, A.; Andreoni, W. *ChemPhysChem*, **2005**, *6*, 1795.

70 Harcourt, R. D. *J. Phys. Chem.* **1991**, *95*, 6916.

71 Zhang, Q.; Lu, X.; Huang, R.; Zheng, L. *Inorg. Chem.* **2006**, *45*, 2457.

72 Rawson, J. M.; Palacio, F. *Struct. Bonding* **2001**, *100*, 93.

73 Cameron, T. S.; Decken, A.; Kowalczyk, R. M.; McInnes, E. J. L.; Passmore, J.; Rawson, J. M.; Shuvaev, K. V.; Thompson, L. K. *Chem. Comm.* **2006**, *21*, 2277.

74 Cameron, T. S.; Lemaire, M. T.; Passmore, J.; Rawson, J. M.; Shuvaev, K. V.; Thompson, L. K. *Inorg. Chem.* **2005**, *44*, 2576.

75 Steudel, R.; Wong, M. W. *Angew. Chem., Int. Ed.* **2007**, *46*, 1768.

76 Drews, T.; Koch, W.; Seppelt, K. *J. Am. Chem. Soc.* **1999**, *121*, 4379.

77 (a) Lyne, P. D.; Mingos, D. M. P.; Ziegler, T. *J. Chem. Soc., Dalton Trans.* **1992**, 2743. (b) Burford, N.; Passmore, J.; Saunders, J. C. P. In Liebman, J. F.; Greenberg, A. (Eds.) *From Atoms to Polymers, Isoelectronic Analogies*, VCH Publishers: Florida, 1989, 53. (c) Burns, R. C.; Gillespie, R. J.; Luk, W.-C.; Slim, D. R. *Inorg. Chem.* **1979**, *18*, 3086.

78 (a) Novoa, J.; Ribas-Arino, J.; Shum, W. W.; Miller, J. S. *Inorg. Chem.* **2007**, *46*, 103. (b) Jung, Y.; Head-Gordon, M. *Phys. Chem. Chem. Phys.* **2004**, *6*, 2008. (c) Jakowski, J.; Simons, J. *J. Am. Chem. Soc.* **2003**, *125*, 16089.

79 Post, B.; Schwartz, R. S.; Fankuchen, I. *Acta Crystallogr.* **1952**, *5*, 372.

80 Cameron, T. S.; Dionne, I.; Jenkins, H. D. B.; Parsons, S.; Passmore, J.; Roobottom, H. K. *Inorg. Chem.* **2000**, *39*, 2042.

81 Cameron, T. S.; Deeth, R. J.; Dionne, I.; Du, H.; Jenkins, H. D. B.; Krossing, I.; Passmore, J.; Roobottom, H. K. *Inorg. Chem.* **2000**, *39*, 5614.

82 Carnell, M. M.; Grein, F.; Murchie, M.; Passmore, J.; Wong, C.-M. *Chem. Commun.* **1986**, 225.

83 (a) Komulainen, J.; Laitinen, R. S.; Suontamo, R. J. *Can. J. Chem.* **2002**, *80*, 1435. (b) Laitinen, R. S.; Pakkanen, T. A. *Inorg. Chem.* **1987**, *26*, 2598. (c) Laitinen, R. S.; Pakkanen, T. A. *J. Chem. Soc., Chem. Commun.* **1986**, 1381.

84 The theoretical treatment of the NMR calculations presented in Section 3.1 is adopted from References 5 and 85.

85 Helgaker, T.; Jaszunski, M.; Ruud, K. *Chem. Rev.* **1999**, *99*, 293.

86 Kutzelnigg, W. Fundamentals of Nonrelativistic and Relativistic Theory of NMR and EPR parameters. In Reference 5.

87 a) Wolinski, K.; Hinton, J. F.; Pulay, P. *J. Am. Chem. Soc.* **1990**, *112*, 8251. b) Ditchfield, R. *Mol. Phys.* **1974**, *27*, 789. c) London, F. *J. Phys. Radium* **1937**, *8*, 397.

88 a) Schindler, M.; Kutzelnigg, W. *J. Chem. Phys.* **1982**, *76*, 1919. b) Kutzelnigg, W. *Isr. J. Chem.* **1980**, *19*, 193.

89 a) Bouman, T. D.; Hansen, A. E. *Chem. Phys. Lett.* **1990**, *175*, 292. b) Hansen, A. E.; Bouman, T. D. *J. Chem. Phys.* **1985**, *82*, 5035.

90 Keith, T. A.; Bader, R. F. W. *Chem. Phys. Lett.* **1992**, *194*, 1.

91 Keith, T. A.; Bader, R. F. W. *Chem. Phys. Lett.* **1993**, *210*, 223.

92 Schreckenbach, G.; Ziegler, T. *Theor. Chem. Acc.* **1998**, *99*, 71.

93 a) Cheeseman, J. R.; Trucks, G. W.; Keith, T. A.; Frisch, M. J. *J. Chem. Phys.* **1996**, *104*, 5497. b) Jaszunski, M.; Helgaker, T.; Ruud, K.; Jørgensen, P.; Bak, K. L.; Koch, H. *Mol. Phys.* **1995**, *85*, 671. c) Van Wüllen, Ch.; Fleischer, U.; Kutzelnigg, W. *Mol. Phys.* **1994**, *81*, 1373. d) Jaszunski, M.; Bak, K. L.; Jørgensen, P.; Helgaker, T.; Ruud, K.; Jensen, H. J. A. *Chem. Phys. Lett.* **1993**, *204*, 608.

94 a) Chan, J. C. C.; Eckert, H. *J. Mol. Struct.(Theochem)* **2001**, *535*, 1. b) Gauss, J. *J. Chem. Phys.* **1993**, *99*, 3629.

95 (a) Wilson, A. K.; Woon, D. E.; Peterson, K. A.; Dunning, T. H., Jr *J. Chem. Phys.* **1999**, *110*, 7667. (b) Woon, D. E.; Dunning, T. H., Jr *J. Chem. Phys.* **1993**, *98*, 1358. (c) Kendall, R. A.; Dunning, T. H., Jr; Harrison, R. J. *J. Chem. Phys.* **1992**, *96*, 6796. (d) Dunning, T. H., Jr *J. Chem. Phys.* **1989**, *90*, 1007.

96 a) Roos, B. O.; Lindh, R.; Malmqvist, P.-Å.; Veryazov, V.; Widmark, P.-O. *J. Phys. Chem. A* **2005**, *109*, 6575. b) Roos, B. O.; Veryazov, V.; Widmark, P.-O. *Theor. Chem. Acc.* **2004**, *111*, 345. c) Roos, B. O.; Lindh, R.; Malmqvist, P.-Å.; Veryazov, V.; Widmark, P.-O. *J. Phys. Chem. A* **2004**, *108*, 2851. d) Pou-Amerigo, R.; Merchan, M.; Nebot-Gil, I.; Widmark, P.-O.; Roos, B. O. *Theor. Chim. Acta* **1995**, *92*, 149. e) Pierloot, K.; Dumez, B.; Widmark, P.-O.; Roos, B. O. *Theor. Chim. Acta* **1995**, *90*, 87. f) Widmark, P.-O.; Persson, B. J.; Roos, B. O. *Theor. Chim. Acta* **1991**, *79*, 419. g) Widmark, P.-O.; Malmqvist, P.-Å.; Roos, B. O. *Theor. Chim. Acta* **1990**, *77*, 291.

97 a) Weigend, F.; Ahlrichs, R. *Phys. Chem. Chem. Phys.* **2005**, *7*, 3297. b) Weigend, F.; Furche, F.; Ahlrichs, R. *J. Chem. Phys*. **2003**, *119*, 12753. c) Schäfer, A.; Huber, C.; Ahlrichs, R. *J. Chem. Phys*. **1994**, *100*, 5829.

98 Autschbach, J. Calculation of Heavy-Nucleus Chemical Shifts. Relativistic All-Electron methods. In Reference 5.

99 a) Pyykkö, P.; Görling, A.; Rösch, N. *Mol. Phys.* **1987**, *61*, 195. b) Edlund, U.; Lejon, T.; Pyykkö, P.; Venkatachalam, T. K.; Buncel, E. *J. Am. Chem. Soc.* **1987**, *109*, 5982.

100 a) Vaara, J.; Malkina, O. L.; Stoll, H.; Malkin, V. G.; Kaupp, M. *J. Chem. Phys.* **2001**, *114*, 61. b) Kaupp, M.; Malkin,V. G.; Malkina,O. L.; Salahub, D. R. *Chem. Phys. Lett.* **1995**, *235*, 382. c) Kaupp, M.; Malkin,V. G.; Malkina, O. L.; Salahub, D. R. *J. Am. Chem. Soc.* **1995**, *117*, 1851; *ibid.* **1995**, *117*, 8492.

101 a) Vaara, J.; Pyykkö, P. *J. Chem. Phys*. **2003**, *118*, 2973. b) Kolb, D.; Johnson, W. R.; Shorer, P. *Phys. Rev. A* **1982**, *26*, 19. c) Feiock, F. D.; Johnson, W. R. *Phys. Rev.* **1969**, *187*, 39.

102 a) Hada, M.; Fukuda, R.; Nakatsuji, H. *Chem. Phys. Lett.* **2000**, *321*, 452. b) Visscher, L.; Enevoldsen, T.; Saue, T.; Jensen, H. J. A.; Oddershede, J. *J. Comput. Chem.* **1999**, *20*, 1262. c) Ishikawa, Y.; Nakajima, T.; Hada, M.; Nakatsuji, H. *Chem. Phys. Lett.* **1998**, *283*, 119.

103 a) Harriman, J. E. *Theoretical Foundations of Electron Spin Resonance*, Academic Press: New York, 1978. b) Pauli, W. Die allgemeinen Prinzipien der Wellenmechanik. In Flügge, S.(Ed.), *Handbuch der Physik*, vol. 5, Springer: Berlin, 1958.

104 a) Kutzelnigg, W. *Z. Phys. D* **1990**, *15*, 27. b) Morrison, J. D.; Moss, R. E. *Mol. Phys.* **1980**, *41*, 491.

105 a) Wolf, A.; Reiher, M.; Hess, B. A. *J. Chem. Phys.* **2002**, *117*, 9215. b) Hess, B. A. *Phys. Rev. A* **1986**, *33*, 3742. c) Douglas, M.; Kroll, N. M. *Ann. Phys.* **1974**, *82*, 89.

106 van Lenthe, E.; Baerends, E. J.; Snijders, J. G. *J. Chem. Phys.* **1993**, *99*, 4597.

107 Wolff, S. K.; Ziegler,T.; van Lenthe, E.; Baerends, E. J. *J. Chem. Phys.* **1999**, *110*, 7689.

108 Kaupp, M. Interpretation of NMR Chemical Shifts. In Reference 5.

109 Kaupp, M.; Malkina, O. L.; Malkin, V. G. *J. Comput. Chem.* **1999**, *20*, 1304, and references therein.

110 (a) Kaupp, M.n; Aubauer, C.; Engelhardt, G.; Klapötke, T. M.; Malkina, O. L. *J. Chem. Phys*. **1999**, *110*, 3897. (b) Kaupp, M.; Malkina, O. L.; Malkin, V. G.; Pyykkö, P. *Chem.–Eur. J.* **1998**, *4*, 118.

111 (a) Kapre, R.; Ray, K.; Sylvestre, I.; Weyhermüller, T.; DeBeer George, S.; Neese, F.; Wieghardt, K. *Inorg. Chem.* **2006**, *45*, 3499. (b) Ray, K.; Weyhermüller, T.; Neese, F.; Wieghardt, K. *Inorg. Chem.* **2005**, *44*, 5345. (c) Hong, G.; Dolg, M.; Li, L. *Chem. Phys. Lett*. **2001**, *334*, 396.

112 (a) Fukuda, R.; Hada, M.; Nakatsuji, H. *J. Chem. Phys.* **2003**, *118*, 1027. (b) Fukui, H.; Baba, T. *J. Chem. Phys.* **2002**, *117*, 7836.

113 Benzi, C.; Crescenzi, O.; Pavone, M.; Barone, V. *Magn. Reson. Chem.* **2004**, *42*, S57.

114 Searles, D. J.; Huber, H. Molecular Dynamics and NMR Parameter Calculations. In Reference 5.

115 Ciofini, I. Use of Continuum Solvent Models in Magnetic Resonance Parameter Calculations. In Reference 5.

116 a) Tomasi, J.; Mennucci, B.; Cancès, E. *J. Mol. Struct. (Theochem)* **1999**, *464*, 211. b) Colominas, C.; Luque, F. J.; Teixidó, J.; Orozco, M. *Chem. Phys.* **1999**, *240*, 253. c) Amovilli, C.; Mennucci, B. *J. Phys. Chem. B* **1997**, *101*, 1051. d) Floris, F. M.; Tomasi, J.; Pascual-Ahuir, J. L. *J. Comput. Chem.* **1991**, *12*, 784.

117 a) Manalo, M. N.; de Dios, A. C.; Cammi, R. *J. Phys. Chem. A* **2000**, *104*, 9600. b) Zhan, C.-G.; Chipman, D. M. *J. Chem. Phys.* **1999**, *110*, 1611. c) Åstrand, P.-O.; Mikkelsen, K. V.; Jørgensen, P.; Ruud, K.; Helgaker, T. *J. Chem. Phys.* **1998**, *108*, 2528. d) Cammi, R. *J. Chem. Phys.* **1998**, *109*, 3185. e) Cremer, D.; Olsson, L.; Reichel, F.; Kraka, E. *Isr. J. Chem.* **1994**, *33*, 369. f) Bühl, M.; Steinke, T.; Schleyer, P. v. R.; Boese, R. *Angew. Chem., Int. Ed. Engl.* **1991**, *30*, 1160.

118 a) Laasonen, K.; Sprik, M.; Parrinello, M.; Car, R. *J. Chem. Phys.* **1993**, *99*, 9080. b) Car, R.; Parrinello, M. *Phys. Rev. Lett.* **1985**, *55*, 2471.

119 Mennucci, B. *J. Am. Chem. Soc.* **2002**, *124*, 1506.

120 Mennucci, B.; Martinez, J. M.; Tomasi, J. *J. Phys. Chem. A* **2001**, *105*, 7287.

121 a) Cossi, M.; Crescenzi, O. *J. Chem. Phys.* **2003**, *118*, 8863. b) Barone, V.; Crescenzi, O.; Improta, R. *Quant. Struct.-Act. Relat.* **2002**, *21*, 105.

122 a) Sterzel, M.; Autschbach, J. *Inorg. Chem.* **2006**, *45*, 3316. b) Autschbach, J.; Zheng, S. *Magn. Reson. Chem.* **2006**, *44*, 989. c) Autschbach, J.; Le Guennic, B. *Chem.–Eur. J.* **2004**, *10*, 2581.

123 Bagno, A.; Rastrelli, F.; Saielli, G. *J. Phys. Chem. A* **2003**, *107*, 9964.

124 Tuononen, H. M.; Suontamo, R.; Valkonen, J.; Laitinen, R. S. *J Phys. Chem. A* **2004**, *108*, 5670.

125 Burns, R. C.; Collins, M. J.; Gillespie, R. J.; Schrobilgen, G. J. *Inorg. Chem.* **1986**, *23*, 4465.

126 Brownridge, S.; Calhoun, L.; Laitinen, R.S.; Passmore, J.; Pietikäinen, J.; Saunders, J. *Phosphorus Sulfur Silicon Relat. Elem.* **2001**, *168/169*, 105.

127 Laitinen, R. S.; Pekonen, P.; Suontamo, R. J. *Coord. Chem. Rev.* **1994**, *130*, 1.

PAPER I

https://doi.org/10.1021/ic049035g

PAPER II

https://doi.org/10.1021/ic061523w

PAPER III

https://doi.org/10.1021/ic048310w

PAPER IV

https://doi.org/10.1021/ic8015673

Brownridge, S.; Calhoun, L.; Laitinen, R. S.; Murchie, M.; Passmore, J.; Pietikäinen, J.; Rautiainen, J. M.; Sanders, J. C. P.; Schrobilgen, G. J.; Suontamo, R. J.; Valkonen, J. U.; Wong, C.-M. "^{77}Se NMR Spectroscopic and DFT MO Investigation of the Reversible Dissociation of $(Se_6I_2)[AsF_6]_2$ in Liquid SO_2." Manuscript.